

**GRAPHENE-COMPLEX OXIDE  
HETEROSTRUCTURE**

by

**Jianan Li**

Bachelor of Science, Hong Kong Baptist University, 2011

Submitted to the Graduate Faculty of  
the Department of Physics in partial fulfillment  
of the requirements for the degree of  
**Doctor of Philosophy**

University of Pittsburgh

2019

UNIVERSITY OF PITTSBURGH  
DEPARTMENT OF PHYSICS AND ASTRONOMY

This dissertation was presented  
by

Jianan Li

It was defended on  
January 16, 2019  
and approved by

Jeremy Levy

Department of Physics and Astronomy, University of Pittsburgh

Vincent Liu

Department of Physics and Astronomy, University of Pittsburgh

Gurudev Dutt

Department of Physics and Astronomy, University of Pittsburgh

Adam Leibovich

Department of Physics and Astronomy, University of Pittsburgh

Xiao Di

Department of Physics, Carnegie Mellon University

Dissertation Director: Jeremy Levy

Department of Physics and Astronomy, University of Pittsburgh

Copyright © by Jianan Li

2019

# **GRAPHENE-COMPLEX OXIDE HETEROSTRUCTURE**

Jianan Li, PhD

University of Pittsburgh, 2019

## TABLE OF CONTENTS

|   |    |
|---|----|
| <b>PREFACE . . . . .</b>                  | xv |
| <b>I. INTRODUCTION . . . . .</b>          | 1  |
| A. LAO/STO heterostructure . . . . .      | 1  |
| 1. STO . . . . .                          | 1  |
| 2. LAO/STO interface . . . . .            | 1  |
| 3. Superconductivity . . . . .            | 1  |
| 4. Magnetism . . . . .                    | 1  |
| B. Graphene . . . . .                     | 1  |
| <b>II. EXPERIMENTAL METHODS . . . . .</b> | 2  |
| A. Sample growth . . . . .                | 2  |
| 1. LAO/STO growth . . . . .               | 2  |
| a. Pre-growth treatment . . . . .         | 2  |
| b. PLD deposition . . . . .               | 3  |
| 2. Graphene growth . . . . .              | 3  |
| a. Copper substrate preparation . . . . . | 7  |
| b. CVD growth . . . . .                   | 12 |
| B. LAO/STO sample processing . . . . .    | 14 |
| 1. Photolithography . . . . .             | 15 |
| a. Spin-coating . . . . .                 | 15 |
| b. UV exposure . . . . .                  | 16 |
| c. Developing . . . . .                   | 20 |
| 2. Ion milling . . . . .                  | 21 |

|  |    |
|--|----|
| 3. Deposition . . . . .  | 24 |
| 4. Lift-off . . . . .  | 24 |
| 5. Oxygen plasma cleaning . . . . .                                  | 26 |
| C. Electronic signal measurement . . . . .                           | 26 |
| 1. Lock-in amplifier . . . . .                                       | 26 |
| 2. Virtual lock-in amplifier . . . . .                               | 26 |
| 3. IV-curve measurement . . . . .                                    | 26 |
| D. Atomic force microscope . . . . .                                 | 26 |
| 1. Working principle . . . . .                                       | 27 |
| 2. Contact mode . . . . .  | 29 |
| 3. AC mode . . . . .   | 30 |
| 4. Non-contact mode . . . . .  | 31 |
| 5. Magnetic force microscopy . . . . .                               | 32 |
| 6. Piezoresponse force microscopy . . . . .                          | 33 |
| 7. LAO/STO nano-device c-AFM lithography . . . . .                   | 35 |
| E. Graphene/LAO/STO device fabrication . . . . .                     | 35 |
| 1. Overview of the Hyflon transfer method . . . . .                  | 41 |
| 2. Hyflon solution preparation and spin-coating . . . . .            | 41 |
| 3. Graphene preparation, copper etching and wet transfer . . . . .   | 41 |
| 4. Photolithography and etching . . . . .                            | 45 |
| a. One-step etching . . . . .  | 45 |
| b. Two-step etching . . . . .  | 47 |
| 5. Graphene/LAO/STO nano-device lithography . . . . .                | 50 |
| <b>III. GRAPHENE P-N JUNCTION EDGE-STATE ENGINEERING . . . . .</b>   | 53 |
| <b>IV. GRAPHENE/LAO/STO SUPERLATTICE DEVICE . . . . .</b>            | 54 |
| <b>V. MAGNETO-OPTICAL KERR EFFECT ON LAO/STO INTERFACE . . . . .</b> | 55 |
| A. Motivation . . . . .  | 55 |
| B. Experimental setup . . . . .                                      | 55 |
| C. Results . . . . .   | 55 |
| <b>VI. OUTLOOK . . . . .</b>   | 56 |

|                            |    |
|----------------------------|----|
| VII. CONCLUSIONS . . . . . | 57 |
| BIBLIOGRAPHY . . . . .     | 58 |

## LIST OF TABLES

|   |  |    |
|---|--|----|
| 1 | Spin-coating conditions for AZ4210 and AZ4110 . . . . .  | 16 |
| 2 | UV exposure and developing conditions for AZ4210 and AZ4110 . . . . .  | 21 |
| 3 | Comparison of etching methods. . . . .   | 22 |
| 4 | One-step RIE etching recipe. . . . .   | 48 |
| 5 | One-step RIE etching recipe. . . . .   | 52 |
| 6 | RIE and barrel etching recipe. Although it seems that the barrel etcher is running at higher power, the structure of the instrument make the etching much less invasive compared to RIE. . . . . | 52 |

## LIST OF FIGURES

|   |  |   |
|---|--|---|
| 1 | PLD epitaxial growth. The PLD chamber is back-filled with oxygen to the target pressure. A beam of pulsed deep-UV excimer laser is focused onto the LAO target. LAO is ablated off and a plume of plasma extends towards the heated substrate on top, and condensed into atomic layer films. RHEED signal is used to monitor the thickness of LAO. . . . .   | 4 |
| 2 | AFM image of the sample after PLD growth and RHEED signal for PLD. (a) shows is the AFM Image. The stripes are the crystal terraces, with $h \approx 4\text{\AA}$ . Inset of a is the raw diffraction sigal of RHEED. (b) is the RHEED signal oscillation during the film epitaxial growth. Each cycle indicates the completion of one unit cell. Adapted from [?]. . . . .  | 5 |
| 3 | Graphene CVD growth. At a temperature $T \approx 1000$ °C, methane molecules will react with copper surface and leave carbon atom on the surface. Carbon atom will self-assemble into graphene due to lattice-match between graphene and copper super-cell. Hydrogen is used to etch away the smaller domain so that the final single layer graphene domains is as large as possible. If the hydrogen is too much, the larger domain will be etched as well. Ratio of methane and hydrogen has to be carefully controlled. . . . . | 7 |
| 4 | Diamond turning machine at work. (a) Copper is fixed onto a turning spindle with vacuum. (b) Mineral spirit is sprayed to the tool and cutting spot, to cool down the surface and blow away the debris. . . . .  | 8 |
| 5 | (a) Diamond cutting tool. (b) Magnified image of the tool tip. The radius of curvature $r = 1.5$ mm. . . . .   | 9 |



|    |   |    |
|----|---|----|
| 10 | Suss UV mask aligner. The mercury lamp generates broad band light from arc. The light is reflected by an ellipsoidal mirror and focused on a cold light mirror, where the UV is selected. The exposure time and dose is controlled by a shutter. The UV is collected by a condenser lens and diffraction reduction optics for collimation and resolution enhancement. Finally, the UV is shed on the sample with a folding mirror and front lens. The sample is in close contact with a mask, where chromium is partially removed. UV exposes the photoresist on sample and print the mask pattern on it. . . . . | 18 |
| 11 | Heidelberg direct laser writer. The sample is illuminated by red light from a diode, and realtime image of sample surface can be monitored with a CCD. UV with $\lambda = 405$ nm is generated from a laser diode. The laser is expanded and filtered, and focused on the sample surface with a high-NA objective. The sample is fixed on a piezo-driven stage. The CCD image, laser power, sample movement and layer alignment are all controlled with computer, so that the laser path and dose control is fully automatic. . . . .   | 19 |
| 12 | Exposed and developed sample. The bright regions are free of photoresist while the rest of the sample is still covered. . . . .   | 20 |
| 13 | Simplified view of ion mill. The argon ions are generated from the discharge chamber on the right hand side. Electrons are extracted from the heated cathode and ionize Ar molecules before they reach the chamber, which works as an anode cup. A magnetic field is applied through a solenoid to increase electrons' path. $\text{Ar}^+$ are accelerated and aligned by the grids to 500 eV. Electrons from the neutralizer are mixed with the $\text{Ar}^+$ plasma flow so that the collimation can be maintained. Sample is tilted by an angle of 22.5°. . . . .  | 23 |
| 14 | E-beam evaporator. The electron beam is generated from an electron gun on the bottom. The beam is deviated and shaped by magnetic field, towards the material. Them material is loaded in a crucible and heated up to melting point. The vapor of the material is thrown towards the sample on top. Deposition time is controlled by a shutter. . . . .   | 25 |

|    |   |    |
|----|---|----|
| 15 | The schematics of AFM. A laser is reflected from the top surface of the AFM tip, and collected by a quad detector. A small amount of deformation would cause the center of laser spot to move on the quad detector, and measured as a change of differential voltage. . . . .   | 28 |
| 16 | The interaction between tip and the sample surface. At long distance the interaction zero. When the tip moves towards the sample, the interaction is attractive. As the tip gets closer, the interaction would switch from attraction to repulsion, and gets larger and larger the tip moves closer. . . . .  | 29 |
| 17 | AFM contact mode. The tip is pressed to the sample surface by the piezoelectric actuator. The deformation of the tip is monitored by the quad detector. The voltage of the piezoelectric actuator is controlled with a feedback loop with the deflection voltage on the quad detector. . . . .  | 30 |
| 18 | AFM AC mode. Left: the tip is driven at a frequency close to the resonance frequency. When the resonance frequency shifts as the interaction between the tip and the sample changes, the Change of oscillation amplitude is monitored by the quad detector and sent to the computer. . . . .  | 31 |
| 19 | AFM Contact mode. The tip is kept at a distance from the sample so that the interaction is always attractive. The tip does not have direct contact with the sample during the scanning. . . . .   | 32 |
| 20 | MFM mode. The first scan is close to the sample surface, so that the topographical information can be obtained. In the second scan the tip is lifted to a constant distance from the sample surface, so that the Van der Waals interaction is negligible and only the long-ranged magnetic interaction is measured.   | 34 |
| 21 | PFM measurement. The external electric field is applied on the sample through a conductive tip. The sample deforms and slightly bend the tip, and the deformation signal is monitored with a quad detector (not shown). If the sample contract in the direction of the field, the deformation signal is in phase with the driving voltage (above); if the sample elongate in the direction of the field, the signal would be out of phase with the driving voltage (below). . . . | 36 |



|    |   |    |
|----|---|----|
| 27 | Contaminants can be introduced by wet transfer. The source can be photoresist, copper etchant, or liquid trapped in the bubble formed from transferring.<br>(a) Contaminants can be seen after graphene transfer. Only the graphene inside the red circles (zoomed-in image in Figure 28) need to be protected with photoresist, and rest of the graphene can be removed along with the contaminants by RIE procedure. (b) Sample surface is clean after RIE procedure. . . . .   | 46 |
| 28 | The graphene area of interest on pre-patterned LAO/STO sample. The patterns are for graphene and LAO/STO interface contact. . . . .   | 47 |
| 29 | Graphene is shaped into Hall bars by RIE. Outside the Hall bar region, nanostructures need to be created inside the square region, on the interface of LAO/STO. Aggressive RIE process can damage the LAO/STO interface. . . . .  | 48 |
| 30 | Two-step graphene etching. . . . .  | 49 |
| 31 | Two-step graphene etching. (a) AZ4210 is spin-coated on Hyflon. (b) The photoresist is patterned into square-shape protection layer for the canvas. (c) An aggressive RIE process is used to fully remove the contaminants outside the canvas. (a) to (c) might be repeated if necessary. (d) AZ4110 is spin-coated. (e) Hall bar shape is patterned, to protect the Hyflon and graphene on the regions of interest. (f) A weak oxygen plasma etching step is used to remove the unwanted Hyflon and graphene. (g) AZ110 is washed off by solvents. (h) Hyflon is removed by FC-40. . . . . | 51 |

## **PREFACE**

I want to thank everyone that made this happened.

## I. INTRODUCTION

### A. LAO/STO HETEROSTRUCTURE

1. STO
2. LAO/STO interface
3. Superconductivity
4. Magnetism

### B. GRAPHENE

## II. EXPERIMENTAL METHODS

### A. SAMPLE GROWTH

#### 1. LAO/STO growth

The properties of LAO/STO interfaces is extremely sensitive to growth conditions such as substrate temperature, background oxygen pressure, annealing conditions, etc[]]. The samples in my experiments are grown with pulsed laser deposition (PLD) by our collaborators at University of Wisconsin-Madison.

**a. Pre-growth treatment** STO (001) substrates are purchased from commercial crystal suppliers. The substrates have a carefully controlled mis-cut angle  $< 0.1^\circ$ , so that the width atomic terraces on STO surface is about 500nm (Figure 2(a)). It has been reported that the terraces on LAO/STO surface can affect the properties of the LAO/STO interface[], therefore we would like the nano-devices located on a single terrace. If the terraces are too wide however, the LAO cannot grow evenly on STO surface during the PLD process due to the high activation energy for atomic migrations, and end up forming holes on the sample (FIG. []).

Before PLD growth, the STO (001) substrates are etched with buffered HF acid to remove SrO and become  $\text{TiO}_2$  terminated. Then they are annealed at  $1000^\circ\text{C}$  for several hours, so that the surface will reconstruct and form crystal terraces[]. Then the samples are etched in HF acid for a second time for a clean surface to start with.

**b. PLD deposition** In PLD deposition, KrF excimer laser ( $\lambda = 248$  nm) pulses are focused on a LAO target and plumes of target material are deposited on the pre-heated STO substrates. Two growth conditions are used for LAO/STO samples: (a) STO substrate is heated at  $T_{\text{STO}} = 550^\circ\text{C}$  and chamber background oxygen pressure  $P(O_2)$  is maintained at  $1 \times 10^{-3}$  mbar, and sample is annealed in 1 atm of  $O_2$  after growth. (b) STO substrate is heated at  $T_{\text{STO}} = 780^\circ\text{C}$  and chamber background oxygen pressure  $P(O_2) = 7.5 \times 10^{-5}$  mbar; sample is annealed at  $T_{\text{STO}} = 600^\circ\text{C}$ ,  $P(O_2) = 300$  mbar for 1 hour after growth, or the so called “Augsburg condition”. Samples grown in condition (a) are used for nano-scale device lithography (i.e. the sub-critical thickness 3.4 uc LAO/STO samples), while condition (b) favors the formation of oxygen vacancies and sample grown in such conditions are used for magnetism experiments[].

Figure 1 illustrates PLD epitaxial growth of LAO. The sample is loaded in an ultra-high vacuum chamber, backed filled with oxygen to the target pressure. Deep UV excimer laser is focused on the LAO crystal target through an optical window on the chamber. The target material is ablated off by the laser and forms a plasma plume. The STO substrate is heated up and placed on top of the target. As the plume expands, target material would condense on the substrate and forms atomic-thin films epitaxially. The high temperature of the substrate facilitates crystallization and epitaxial growth of the target material.

During the PLD growth, the reflection high-energy electron diffraction (RHEED) is used for *in-situ* monitoring the thickness of epitaxial layers. A beam of electron is generated from a source and reflected from the substrate as the film growth. Electron diffraction signal is collected by a detector on the other side (Figure 2(a) inset). The intensity of the diffraction oscillates as a function of film thickness. The thickness of LAO can be precisely controlled by counting the cycles of RHEED signal (Figure 2(b)).

## 2. Graphene growth

The two most popular methods to obtain single-layer/few-layer graphene are mechanical exfoliation and chemical vapor deposition (CVD).

The mechanical exfoliation isolate single layer graphene directly with adhesive tapes.

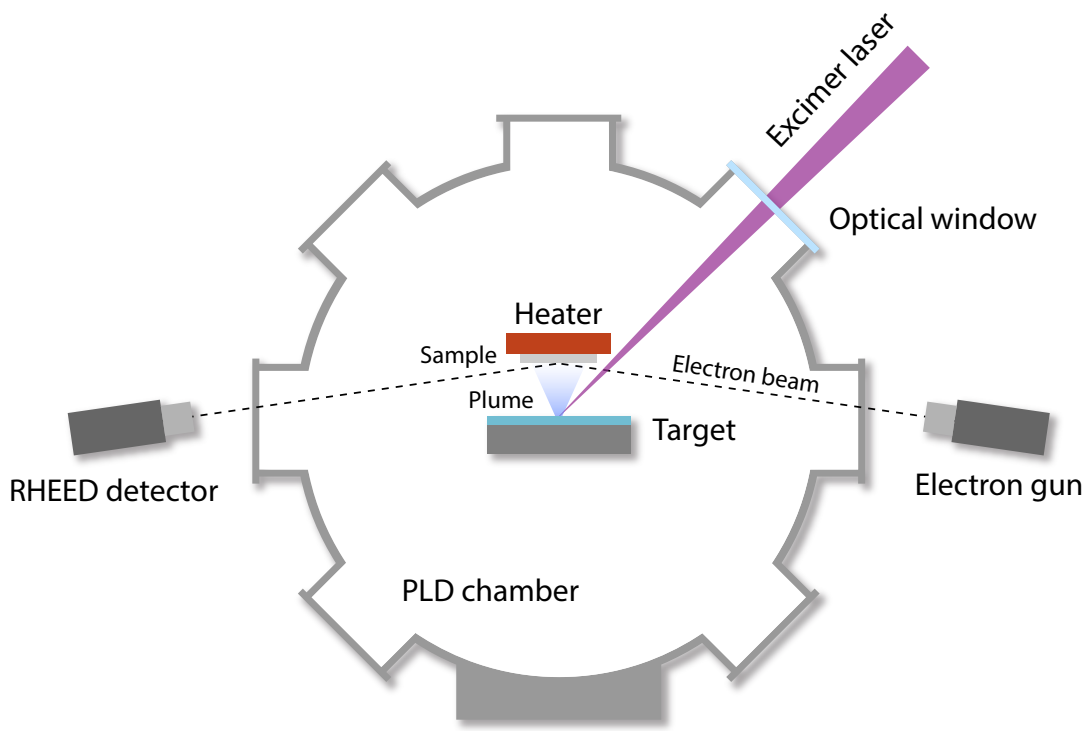
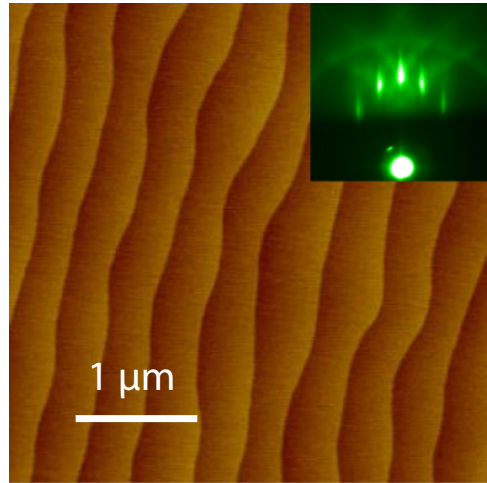
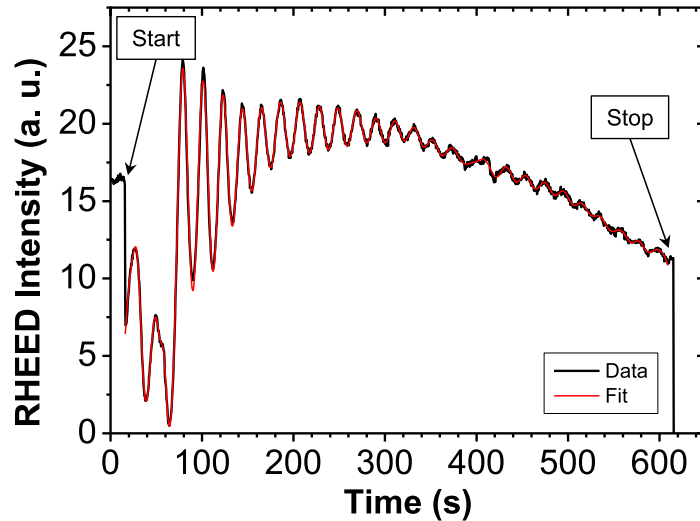


Figure 1: PLD epitaxial growth. The PLD chamber is back-filled with oxygen to the target pressure. A beam of pulsed deep-UV excimer laser is focused onto the LAO target. LAO is ablated off and a plume of plasma extends towards the heated substrate on top, and condensed into atomic layer films. RHEED signal is used to monitor the thickness of LAO.



(a)



(b)

Figure 2: AFM image of the sample after PLD growth and RHEED signal for PLD. (a) shows is the AFM Image. The stripes are the crystal terraces, with  $h \approx 4\text{\AA}$ . Inset of a is the raw diffraction sigal of RHEED. (b) is the RHEED signal oscillation during the film epitaxial growth. Each cycle indicates the completion of one unit cell. Adapted from [?].

Graphene is a type of Van der Waals material, which means that the carbon atoms within a layer are tightly bonded with covalent bond while the layers are bonded by the much weaker Van der Waals force. Adhesive tapes can easily separate graphene layers. After multiple exfoliation steps, single layer graphene flakes can be separated and identified<sup>[1]</sup>. One key aspect of the exfoliation method is choosing a proper substrate so that single layer graphene can be easily identified with optical microscopes. Although graphene has the highest absorption coefficient in the visible light regime<sup>[2]</sup>, spotting a single layer graphene flake on a transparent substrate is still challenging, and is always assisted with other characterization methods such as Raman spectroscopy<sup>[3]</sup> to ensure the graphene is single layer. The most commonly used substrate is silicon wafer with 400 nm thick silicon oxide coating. The graphene on SiO<sub>2</sub> surface modifies the interference of visible light between the top and bottom layer of the coating, and make graphene layers distinguishable<sup>[4]</sup>.

CVD is another method to obtain single layer graphene. Graphene flake from mechanical exfoliation is mostly a few micrometers or tens of micrometers; the size and shape cannot be well controlled. CVD on the other hand, can grow continuous graphene of wafer sizes<sup>[5]</sup>, and then etch it into any desired shapes through post processing.

The CVD process uses gaseous organic molecules (methane, ethylene, etc) as carbon source, and graphene lattice-matching crystal such as SiC, Ni and Cu as substrate. In high temperature (about 1000 °C), the metal surface has highly reactive and can serve as a catalyst, so the gas molecules will react with the surface and carbon atoms are detached. At the high temperature, the carbon atoms will self-assemble into graphene. Over the entire process the substrate is in continuous gas flow so the gaseous byproducts are flushed away. Hydrogen is used to assist the growth. Without hydrogen molecules, graphene will grow simultaneously on the entire surface and form many small domains. Hydrogen will etch away the smaller domains while the larger domains are growing<sup>[6]</sup> until the domains meet or the process is terminated. If the hydrogen portion is too high however, the larger graphene domains will also be etched. CVD is a dynamic process of etching and growth. The ratio of methane and hydrogen need to be carefully controlled.

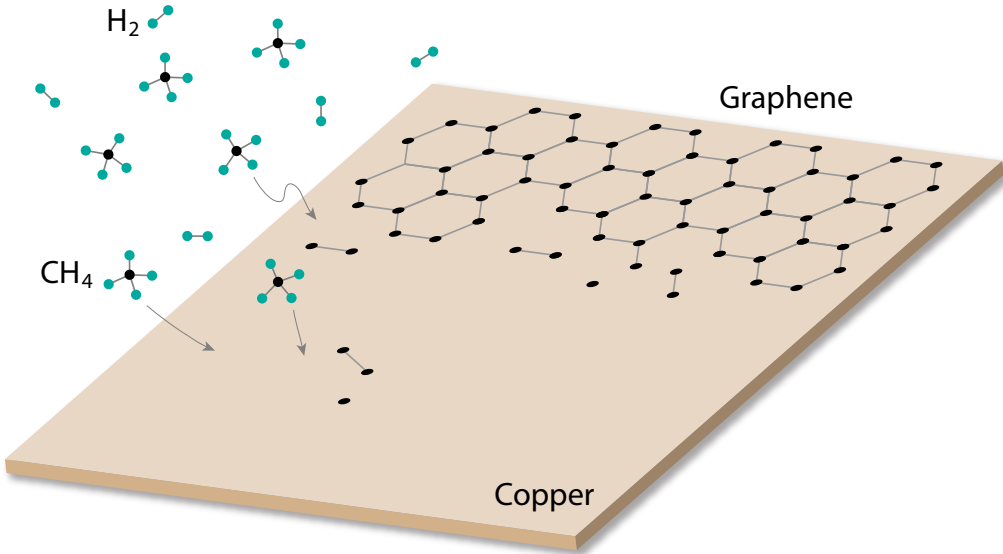


Figure 3: Graphene CVD growth. At a temperature  $T \approx 1000$  °C, methane molecules will react with copper surface and leave carbon atom on the surface. Carbon atom will self-assemble into graphene due to lattice-match between graphene and copper super-cell. Hydrogen is used to etch away the smaller domain so that the final single layer graphene domains is as large as possible. If the hydrogen is too much, the larger domain will be etched as well. Ratio of methane and hydrogen has to be carefully controlled.

**a. Copper substrate preparation** Various materials are used for graphene growth, most commonly SiC, Ir, Ni and Cu. Cu is the most common choice due to the low carbon solubility scalability[?]. Compared to other substrate materials, copper is also easy to be etched with wet chemicals. In CVD growth, the carbon atoms form into graphene following the shape of the substrate. Therefore, the graphene quality is directly related to the substrate. Surface roughness and contaminants on copper provide nucleation centers for graphene, and can cause polycrystalline structure and multi-layer growth[?]. The is-

sue of surface roughness can be addressed with electrochemical polishing[?], or mechanical polishing. In my experiment I used a graphene substrates polishing procedure developed by Dr Brian D'Urso's graduate students, by using diamond turning machine to reduce the roughness from several hundred of nanometer to a few nanometers[?]. Compared to electro-chemically polished substrates, this method can produce surface 50 time smoother and the copper domain sizes are 5 time larger.

Diamond turning machine (DTM) is commonly used for high precision manufacturing, such as laser reflective mirrors. The DTM works like a lathe, where the workpiece is fixed on a turning spindle, and the cutting tool approaches the workpiece and shape or polish the surface by steps. Figure 4 shows the DTM at work. The cylindrical metal piece in 4(a) is the spindle of DTM. Copper piece is fixed on the spindle by vacuum and spins at 2000 rpm. The diamond tool approaches the copper surface from the opposite side. 4(b) is an image taken in the middle of a cutting step. Mineral spirit is sprayed from a nozzle from the left, cools down the surface and blow away the metal debris to the right. Reflection of the tool shows a flat finishing.

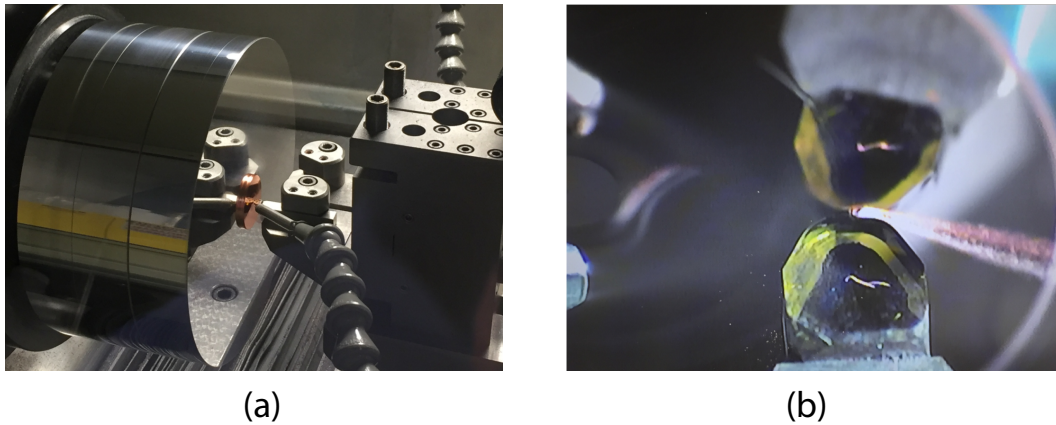


Figure 4: Diamond turning machine at work. (a) Copper is fixed onto a turning spindle with vacuum. (b) Mineral spirit is sprayed to the tool and cutting spot, to cool down the surface and blow away the debris.

Instead of using high-speed-steel tool, the DTM uses a curved-edge (radius of curvature  $r = 1.5$  mm) diamond tool for cutting (Figure 5). By reducing the incremental step to 10  $\mu\text{m}$ , as shown in Figure 6, the roughness of the finishing surface can be smaller than 2 nm. The diamond tool sometimes have dents on the surface, which can leave a trace after each revolution.

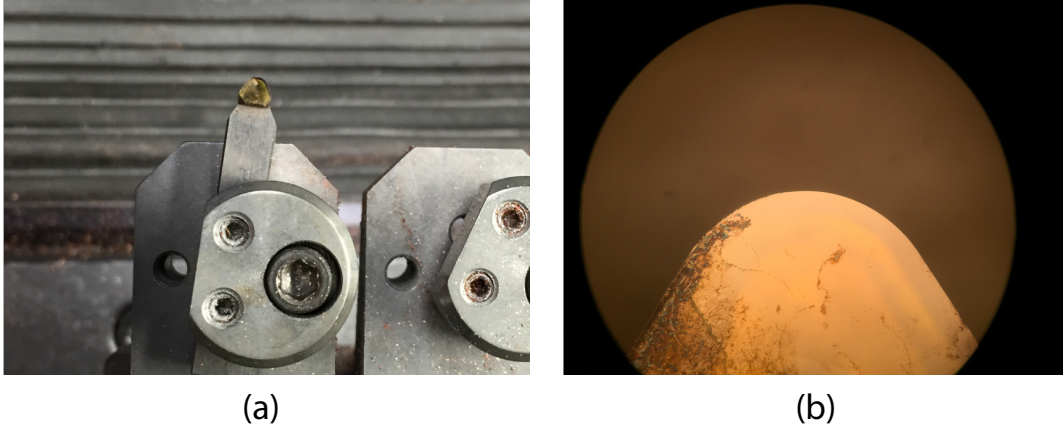


Figure 5: (a) Diamond cutting tool. (b) Magnified image of the tool tip. The radius of curvature  $r = 1.5$  mm.

Other than surface roughness, the copper domain size is another limiting factor for large single domain graphene growth. Although it was not clear the effect of copper substrate domains on the graphene quality[?, ?, ?], larger copper domain sizes gives us a chance to grow larger graphene single crystals. Annealing the copper at high temperature will reconstruct and merge the polycrystalline domains into larger domains, but mechanical processing will introduce defects and break the single domains, therefore the substrate needs to be re-annealed several times before graphene growth starts.

The procedure of making copper rods into copper foils for graphene growth is shown in Figure 7. 1' long oxygen-free high thermal conductivity copper (OFHC) rods with ultra high purity (99.99%) are purchased from McMaster Carr. The rod is first annealed at  $T = 1050^\circ\text{C}$  for 24 h, and the polycrystalline domains will merge into larger domains within the rod. Then

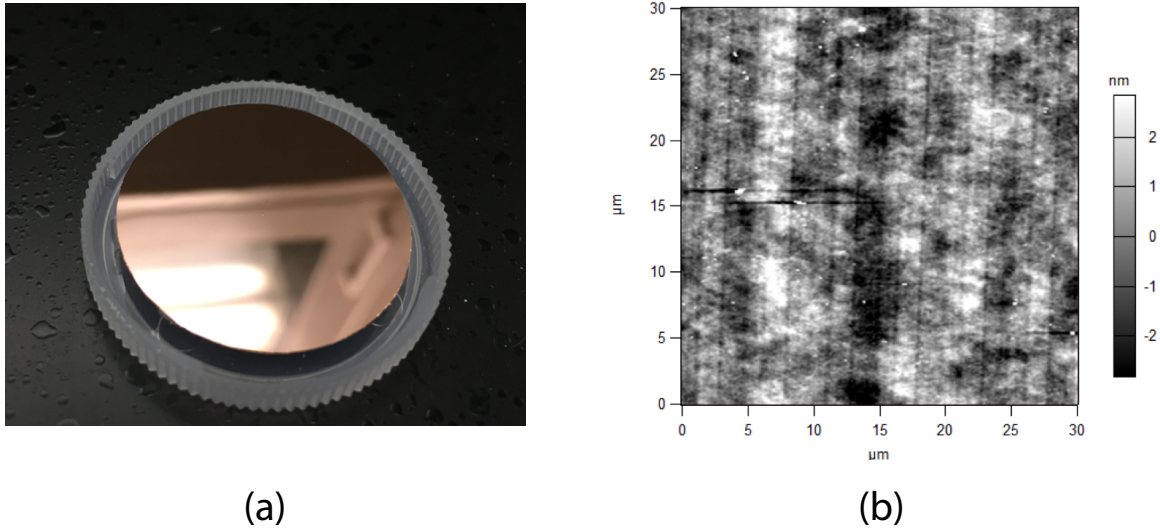


Figure 6: (a) The copper foil after DTM thinning and polishing. The final thickness is about  $100 \mu\text{m}$ . (b) The AFM image of the copper foil surface. The roughness is within 2 nm. Some nanoscale particles can be seen. They will serve as nucleation centers for graphene CVD growth. Reducing the density of surface contaminants will reduce the density of nucleation centers and enlarge the domain size. The vertical grooves are left by the dents on the diamond tool for each revolution. The spacing between grooves is the same as the approaching speed of the tool towards the center. The copper is annealed at  $T = 1050^\circ\text{C}$  for another time before growth starts and the surface will reconstruct, possibly remove those grooves.

the rod is cut into copper discs of 2 mm thick in the machine shop. The mechanical cutting process will break the domains and introduce surface contaminant, so the surfaces copper discs are cleaned on the DTM, and then annealed again at  $1050^\circ\text{C}$  for 8 h. After annealing, the domain re-formation in the disc will cause corrugation on the surface. Therefore, the copper surface is cut with DTM for a second time. Then the copper discs are cut into  $100 \mu\text{m}$  foils, by  $10\mu\text{m}$  steps. During the thinning procedure, the copper will expand on the cutting face and cause deformation, and eventually break the vacuum sealing between the disc and spindle on the backside. Therefore the copper disc needs to be flipped several times

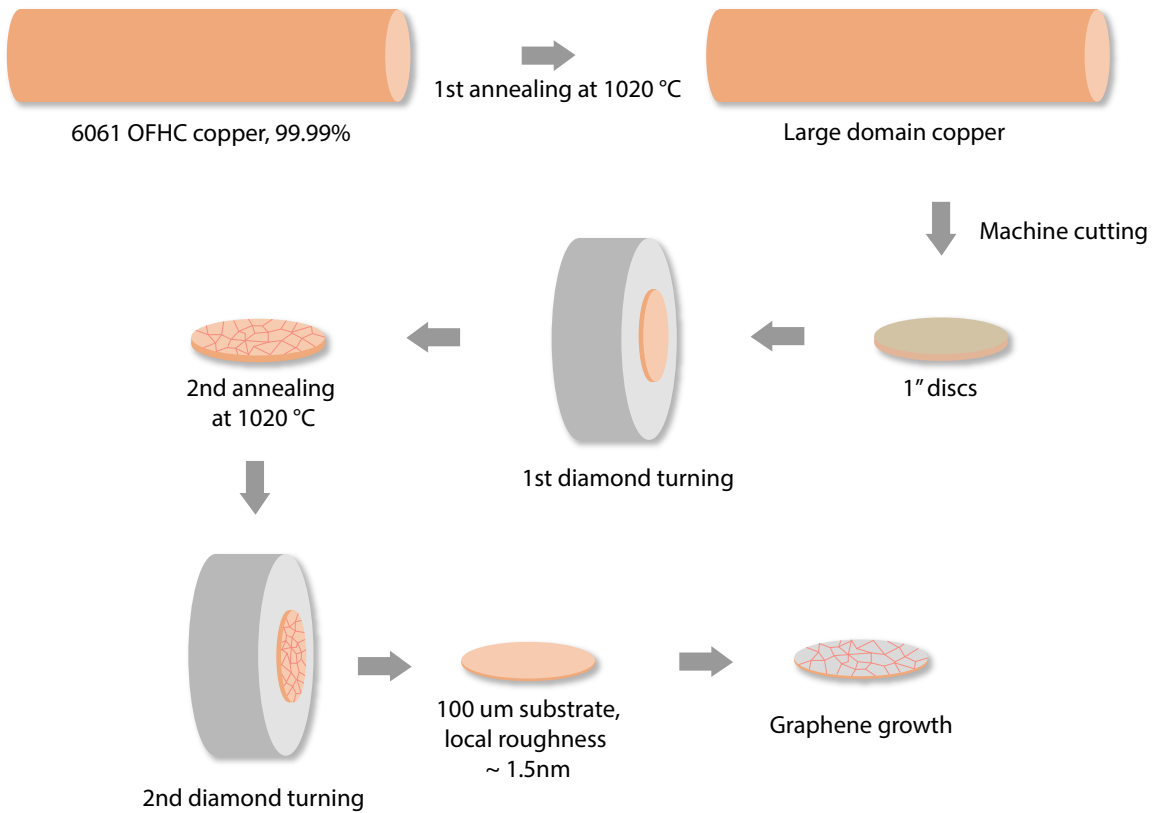


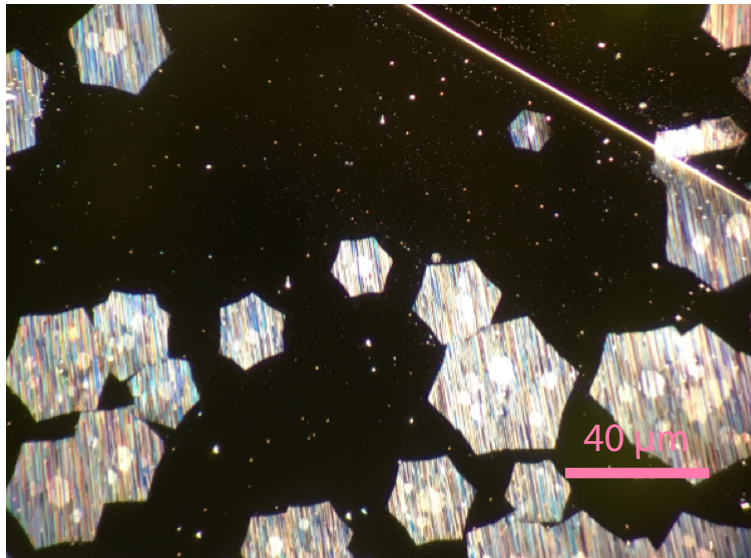
Figure 7: Procedure of cutting copper rods into  $100\mu\text{m}$  foils for graphene growth. High purity OFHC copper rods are purchased from McMaster Carr. The rod is first annealed at  $1050^\circ\text{C}$  for 24 h so that the polycrystalline domains merge into larger domains. Then the rod is cut into 2 mm thick copper discs in the machine shop. The discs are cleaned with DTM and then annealed again to “heal” the domains broken by the mechanical cutting. Domain re-formation would cause surface corrugation, therefore the copper disc surface is cleaned with DTM and then cut into  $100 \mu\text{m}$  foils and ready for graphene CVD growth.

to balance out the expansion and keep it flat when thinned from 2 mm to 100  $\mu\text{m}$ . The process takes about 5 h.

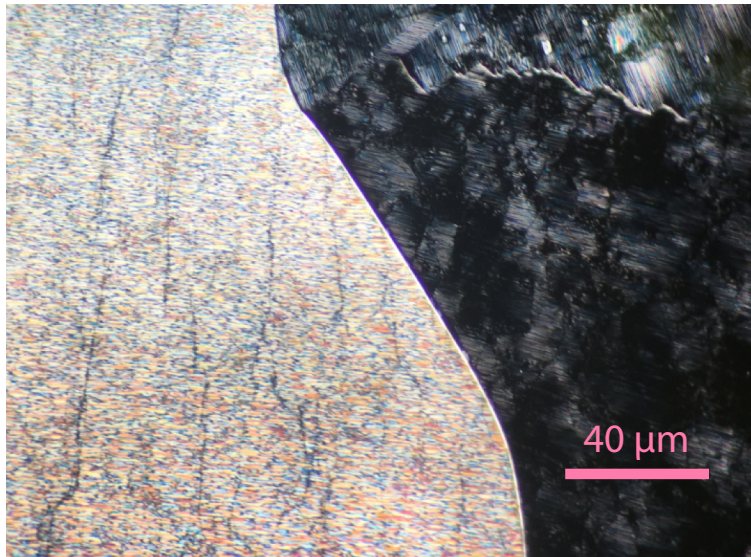
**b. CVD growth** The CVD graphene growth can be performed in low pressure (LPCVD) or atmospheric pressure (APCVD). LPCVD grows graphene at a pressure lower than 100 mTorr, in continuous flow of pure hydrogen and methane and 1000 °C substrate temperature. The problem with LPCVD is that the melting point of copper ( $T_m = 1085^\circ\text{C}$ ) is close to the growth temperature. As a result, the copper will evaporate severely and contaminate the furnace[?]. Also the pure precursor gases bring fire hazard. APCVD can eliminate those difficulties associated with the low pressure and improve the graphene quality[?, ?]. Instead of using pure hydrogen and methane, APCVD uses gas mixture of 2.5 vol % H<sub>2</sub>, balance Ar and 0.1 vol % CH<sub>4</sub>, balance Ar. The furnace is pumped into low vacuum, and then backfilled with hydrogen and methane mixture with argon to atmospheric pressure. The pressure from argon will suppress the evaporation of copper at annealing and growth temperature. The growth procedure are as follows[?].

- The furnace is pumped down to  $\sim 10$  mTorr.
- Backfill the furnace with H<sub>2</sub>/Ar mixture at 186 sccm, up to  $\sim 100$  Torr.
- Start the furnace temperature controller to ramp up to  $T = 1050^\circ\text{C}$ , and let the furnace stay at this temperature for 1 h.
- Start flowing mixture of CH<sub>4</sub>/Ar at 14 sccm into the furnace, and let the copper foil stay in graphene CVD growth condition for 1.5 h.
- Cool down the system to room temperature. The flow of CH<sub>4</sub>/Ar mixture is turned off at  $\sim 650^\circ\text{C}$ . H<sub>2</sub>/Ar mixture keeps flowing overnight until the system is below 50°C.

In Figure 8 the dark-field mode of optical microscope clearly shows the CVD graphene on copper substrates. In 8(a) the copper substrate is partially covered with graphene. Growth process was terminated before graphene fully covered the substrate. Hexagonal shape of single domain graphene flakes can be identified. Some double layer can also be observed. On the top right corner of 8(a) a copper domain boundary can also be identified. 8(b) is the image of graphene grown in another run. The substrate is fully covered with graphene.



(a)



(b)

Figure 8: Dark field mode microscope images of CVD graphene on copper substrates. (a) The copper substrate is partially covered with graphene. Hexagonal shape single domain graphene can be observed. Growth was terminated before graphene fully covered the substrate. (b) Graphene covers the entire copper substrate. Copper domains of two different orientations can be observed.

The image shows two copper domains with different orientations, and therefore the graphene grown on the two domains look different. Wrinkles on graphene can be observed, resulting from different thermal expansion coefficient of copper and graphene.

## B. LAO/STO SAMPLE PROCESSING

One of the challenges with experiments on LAO/STO interface is to make good electrical contact from the bonding pads to the interface. A major part of my research is process the samples before the c-AFM writing can be performed, or graphene can be transferred. The processing methods have to be carefully chosen, so that the 2DEG and interface switchability will not be affected. Sample cleanliness is another concern. Any nano-particles introduced in the processing would affect sample quality, considering that the dimensions of devices are also nanoscale. The procedure has those steps. Details of each steps can be found in the following subsections.

- **Initial cleaning:** the sample is cleaned with acetone and isopropanol alcohol (IPA) in ultrasonic cleaner so that the particles introduced in shipping are cleaned. Usually we do not use deionized-water (DI-water) for cleaning. Proton from the water can get adsorbed on sample surface and affect the interface [].
- **Photolithography:** the sample is patterned with standard UV photolithography procedures, either with optical mask and UV lamp or with direct laser writer, for further processing. The finest features in my design are  $2 \mu\text{m}$  wide.
- **Ion milling:** after the desired patterns are developed on the photoresist, the sample is bombarded with  $\text{Ar}^+$  ion flow so that the LAO/STO interface is exposed for electrical contact.
- **Deposition:** titanium and gold are used for making contact with the exposed LAO/STO interface either by electron-beam evaporation or sputtering.
- **Lift-off:** the excessive metal outside the patterns are removed by the lift-off process following the metal deposition. Like the initial cleaning process, we use IPA and acetone and do not use water as solvent.

- **Oxygen plasma cleaning:** the sample is covered with residue from liquid and photoresist, until it is cleaned with oxygen plasma cleaner. Then the atomic steps can be seen with AFM.

The sample processing procedures are shown in FIG. ??.

## 1. Photolithography

Photolithography is a commonly used technology in semiconductor industry. The substrate is covered with a thin layer of photosensitive material, and exposed under UV with designed pattern. UV would change the solubility of photoresist, and the pattern can be developed in buffered base solution after exposure. The modern state-of-the-art photolithography technology can reach resolution of 10 nm, and is the pillar of support for the semiconductor industry. There are two types of photoresists: positive and negative. Positive photoresist will be washed off after been exposed to UV, while negative photoresist is stabilized by UV and the unexposed parts are removed by developers. In my experiment, three types of positive photoresists are used: AZ4620, AZ4210 and AZ4110. For each sample, a 3" carrier wafer is used as a fixture, because dimensions of the sample (5 mm × 5 mm × 1 mm) is non-standard and most photolithography instruments are designed for 3" or 4" wafer in the university facility. AZ4620 is used to fix the sample to the carrier wafer during spin-coating, exposure and other steps, as a cleanroom-safe "epoxy".

a. **Spin-coating** There are two limiting factors of the feature resolutions in photolithography: diffraction limit of light and photoresist thickness. Spin-coating is a standard technique to keep the photoresist thin and uniformly covering the sample surface. When the sample is spinning at a speed between 1000 rpm and 6000 rpm, the photoresist solution on sample surface would spread out. The liquid will be finally in equilibrium of viscosity, roughness of sample surface and centrifugation from spinning. After the spin-coating the sample is baked at a temperature around 100°C to vaporize the remaining solvent in photoresist and stabilize the film before UV exposure. In my experiment, the spinning speed is 4000 rpm. Thickness of AZ4210 and AZ4110 are 2.1  $\mu\text{m}$  and 1.1  $\mu\text{m}$ , respectively. These two types

| Photoresist        | AZ4210            | AZ4110            |
|--------------------|-------------------|-------------------|
| Spinning speed     | 4000 rpm          | 4000 rpm          |
| Spinning time      | 30 s              | 30 s              |
| Baking temperature | 95 °C             | 95 °C             |
| Baking time        | 60 s              | 60 s              |
| Thickness          | 2.1 $\mu\text{m}$ | 1.1 $\mu\text{m}$ |

Table 1: Spin-coating conditions for AZ4210 and AZ4110

of photoresists have the same chemical composition. They have different concentrations so they end up with different thickness at the same speed. Usually thinner films will have more stable performances for fine features (2  $\mu\text{m}$ , to be specific). In the cases where photoresists are consumed in the processing, such as reactive ion etching, thicker photoresist will be a better option.

The spin-coating conditions are listed in Table 1.

**b. UV exposure** The UV exposure is to use short wavelength photon to change the solubility of photoresist, so that the following developing step can selectively remove the photoresist. Like all optical system, the resolution of exposure is limited by diffraction limit of light. Historically, mercury gas-discharge lamp is used, and 436 nm (“g-line”), 405 nm (“h-line”) and 365 nm (“i-line”) are selected as UV source. Besides Hg lamp, solid state laser and excimer laser with shorter wavelengths are also commonly used UV source. Samples are exposed with two different methods: mask exposure and direct laser writing.

Mask exposure is performed by a mask aligner (Suss MJB3 or MA6, see Figure 10). Incoherent and collimated UV is generated from a Hg lamp and an area of 4”  $\times$  4” is exposed with UV at constant intensity of 10 mW/cm<sup>2</sup>. The sample is covered with a photomask (Figure 9), a square piece of soda glass (to reduce UV absorption) coated with chromium on one side. The desired pattern is pre-printed on the chromium by chemical etching. The patterns on photoresist will be the copy of the patterns on the photomask.

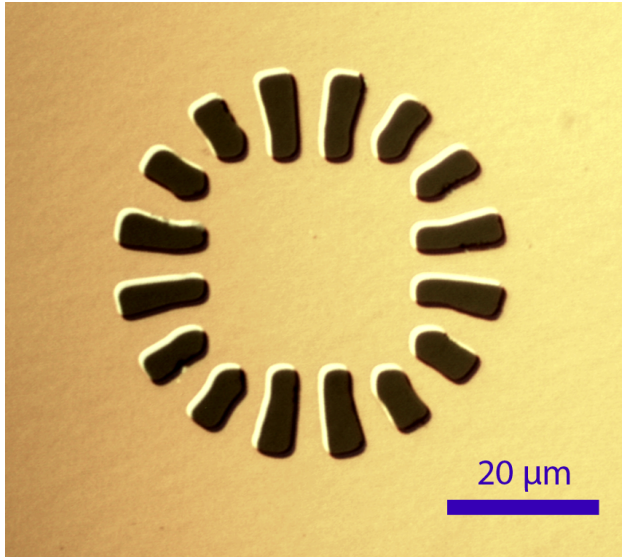


Figure 9: Mask for photolithography. The dark parts are transparent, while the bright parts are covered with chromium. Sample will be exposed where UV is not blocked by chromium. The figure shows the electrodes of a canvas for writing. The pedal shape area to be exposed will be etched away on the sample, and filled with titanium and gold to make contact with the LAO/STO interface.

Direct laser writing uses focused laser beam to write micro-patterns directly on photoresist, without using a mask. This is usually how the photomask is manufactured, but it can also be used to pattern samples. In my experiment I use Heidelberg MLA100 (Figure 11), with 405 nm wavelength UV generated from a solid state laser. The laser is expanded and filtered with a pinhole, and focused on the sample with a high-NA objective. The focusing objective is fixed, and the sample is placed on a piezostage controlled with computer, to follow the designed pattern. The UV dose is determined by both the laser power and laser spot dwell time. It is important to keep the sample surface horizontal, so that laser spot will not defocus while moving through the entire sample surface. Sometimes, especially when the critical dimension is close to  $2 \mu\text{m}$ , the photoresist patterns are not evenly developed, and it is caused by sample tilting and laser defocussing. Focusing quality can be checked with a real-time CCD image, while the sample is illuminated with red light from a second diode.

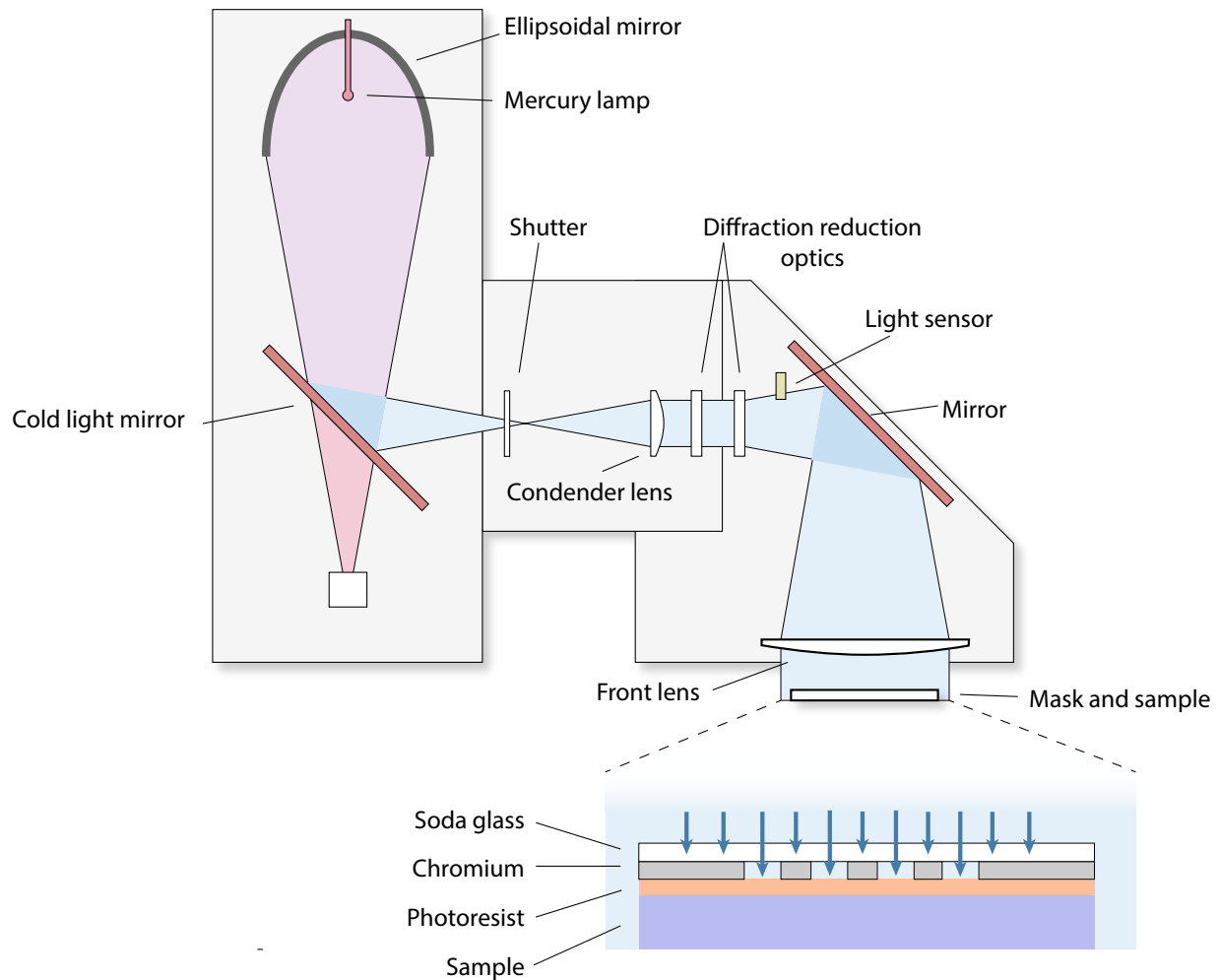


Figure 10: Suss UV mask aligner. The mercury lamp generates broad band light from arc. The light is reflected by an ellipsoidal mirror and focused on a cold light mirror, where the UV is selected. The exposure time and dose is controlled by a shutter. The UV is collected by a condenser lens and diffraction reduction optics for collimation and resolution enhancement. Finally, the UV is shed on the sample with a folding mirror and front lens. The sample is in close contact with a mask, where chromium is partially removed. UV exposes the photoresist on sample and print the mask pattern on it.

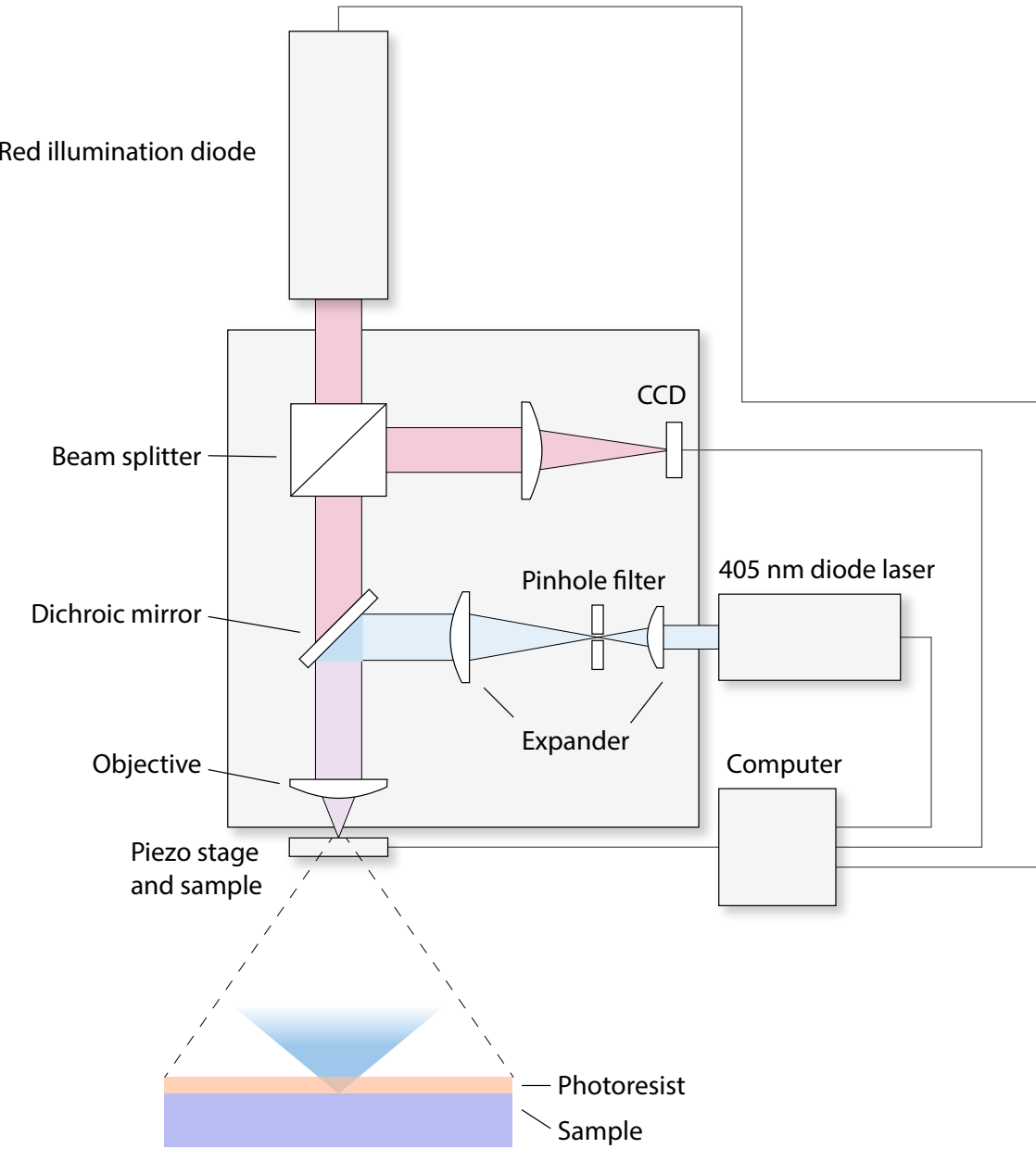


Figure 11: Heidelberg direct laser writer. The sample is illuminated by red light from a diode, and realtime image of sample surface can be monitored with a CCD. UV with  $\lambda = 405$  nm is generated from a laser diode. The laser is expanded and filtered, and focused on the sample surface with a high-NA objective. The sample is fixed on a piezo-driven stage. The CCD image, laser power, sample movement and layer alignment are all controlled with computer, so that the laser path and dose control is fully automatic.

**c. Developing** Developing is the process using buffered base solution to washed away the unwanted parts of photoresist after exposure and reveal the pattern on sample, for future processing steps. Depending on the type of photoresist, either the exposed parts (positive photoresist, such as AZ4210) or unexposed parts (negative photoresist, such as AZ5214) are removed. In my experiment I use AZ400K (potassium borate) for developing. The developer is diluted with DI-water, by 1:3 or 1:4 ratio. Different concentration will maintain different pH level and developing speed. The sample is washed with DI-water after developing, to remove the excessive developer.

A picture of sample after UV exposure and developing is shown in Figure 12. Photoresist in the bright area are washed away while the rest of the sample is still covered with photoresist. Note that the edges of the pattern are less sharp than the mask, because of the resolution limit from diffraction.

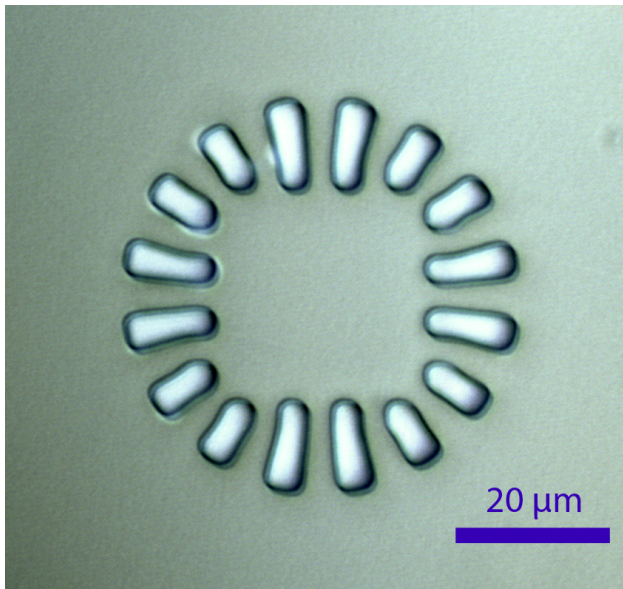


Figure 12: Exposed and developed sample. The bright regions are free of photoresist while the rest of the sample is still covered.

The conditions for exposure and developing are listed in Table 2.

Photolithography is the part that has the most uncertainty in the entire processing, and can affect some samples (like graphene/LAO/STO) more significantly. This will be discussed

| Photoresist       | AZ4210              | AZ4110          |
|-------------------|---------------------|-----------------|
| UV Dose           | 170 mJ              | 100 - 120 mJ    |
| Developer : Water | 1 : 4               | 1 : 4           |
| Developing time   | 120 - 180 s         | 120 - 180 s     |
| Resolution        | 3 - 5 $\mu\text{m}$ | 2 $\mu\text{m}$ |

Table 2: UV exposure and developing conditions for AZ4210 and AZ4110

in future sections.

## 2. Ion milling

LAO/STO interface is buried underneath LAO, so if contact need to make with the interface the LAO has to be etched. Usually there are three methods for etching: wet chemical etching, dry plasma etching and ion milling. Wet chemical etching using reactive chemical solutions (such as HF, HCl) to etch away the materials. This is cheaper but less controlled, and etching is isotropic. Plasma etching, uses the plasma or free radicals of active gas molecules (such as O<sub>2</sub>, SF<sub>6</sub>, etc) to react and remove materials, at pressure between 0.1 and 5 Torr. It is better controlled in etching rate and directionality, but the instrument is more expensive, and finding the right gas to selectively etch the target material while keeping the protecting layer intact is not always feasible. Although there are mature industrial solutions for silicon, alumina and silica etching with plasma, there is not a good solution to etch complex oxides like LAO/STO with our facility plasma etcher. Ion mill uses accelerated ionized argon plasma to physically bombard sample. The etching rate is slower than the previous two methods, but performs well on most inorganic materials including LAO/STO. Also, the etching is more directional. In Table 3 is a comparison of the three etching methods.

Ion mill accelerates Ar ions to a certain kinetic energy and physically etch samples with bombardment. As shown in Figure 13, Ar<sup>+</sup> is generated from the discharge chamber. The entire chamber is pumped to high vacuum ( $< 10^{-6}$  Torr), and back filled with Ar gas to

| Method          | Chemical etching | Plasma etching       | Ion milling              |
|-----------------|------------------|----------------------|--------------------------|
| Cost            | low              | high                 | high                     |
| Directionality  | anisotropic      | anisotropic          | isotropic                |
| Selectivity     | high             | high                 | low                      |
| Speed control   | poor             | good                 | good                     |
| Target material | inorganic        | organic or inorganic | inorganic                |
| Environment     | aqueous, ambient | 0.1 - 5 Torr, vacuum | $< 10^{-4}$ Torr, vacuum |

Table 3: Comparison of etching methods.

$10^{-4}$  Torr. On the right-hand-side of the figure, a filament is heated up and a biased voltage is applied between the filament and chamber wall. Electrons are extracted from the filament and ionize the argon molecules. Usually a magnetic field is applied through a solenoid to increase the path and ion yield before the electrons reach the chamber wall. At the opening side of the discharge chamber, there are two or three layers of electrically isolated screen grids (made of sputter-resisting materials like Mo or W). A voltage of 500eV is applied between the grids so that  $\text{Ar}^+$  can be accelerated to the same energy. The pores on the grids are aligned so that the  $\text{Ar}^+$  flow is collimated. Right after the  $\text{Ar}^+$  exits the chamber, it is mixed with free electrons from a neutralizer filament, so that flow will not be diverged by coulomb attraction between  $\text{Ar}^+$  before they reach the sample. The sample is  $20^\circ$  to  $30^\circ$  off the normal direction, to create undercut and facilitate electrical contact between the interface and the electrodes. The kinetic energy of the plasma is converted to heat on the sample surface. Either the sample is cooled down with flowing water inside the chuck, or the plasma flow is shutoff with a duty cycle so that the sample can cool down by radiation. Temperature over  $150^\circ \text{C}$  will cause phase transition of the photoresist on the sample, and make hard to remove by lift-off.

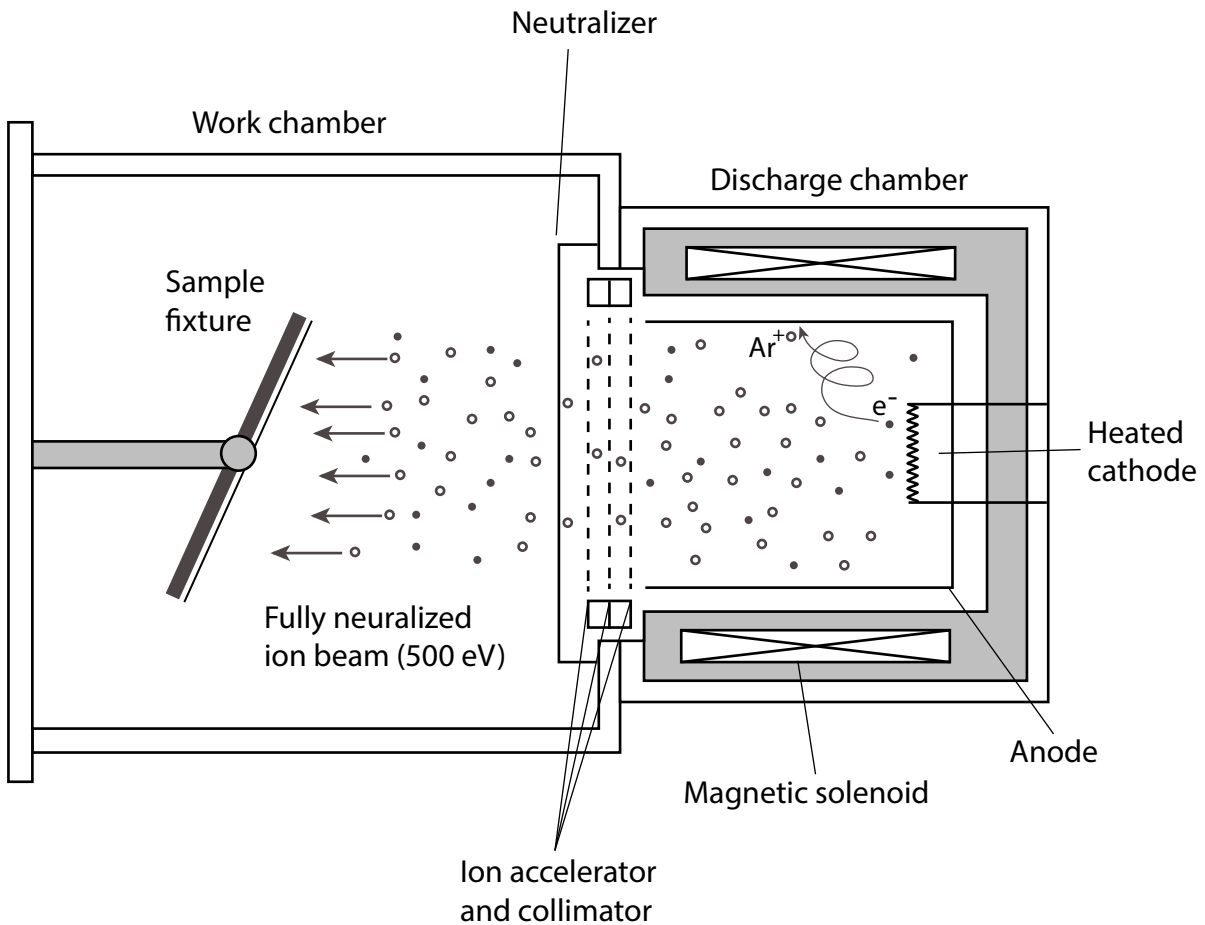


Figure 13: Simplified view of ion mill. The argon ions are generated from the discharge chamber on the right hand side. Electrons are extracted from the heated cathode and ionize Ar molecules before they reach the chamber, which works as an anode cup. A magnetic field is applied through a solenoid to increase electrons' path.  $Ar^+$  are accelerated and aligned by the grids to 500 eV. Electrons from the neutralizer are mixed with the  $Ar^+$  plasma flow so that the collimation can be maintained. Sample is tilted by an angle of 22.5°.

### 3. Deposition

Titanium and gold are used for making contact with the interface of LAO/STO. I use two methods to deposit the material: sputtering and electron-beam (e-beam) evaporation. Sputtering is similar to ion milling, but instead of using  $\text{Ar}^+$  plasma flow to bombard and etch the sample, it is directed towards the target materials (Ti, Au, etc). The binding energy of the target material atoms is much smaller than the kinetic energy of  $\text{Ar}^+$ , and are ejected from the target and deposit onto the sample surface. E-beam evaporation (Figure 14) controls electron-beam to heat up the target material and vaporize it. The vapor is thrown through a long distance ( $> 10 \text{ cm}$ ) before it reaches the sample. Compared to sputtering, the e-beam evaporation is more directional, because of the long throw-distance of evaporated material, compared to sputtering.

As can be seen in Figure 14, a beam of electron is accelerated by a high voltage of 10 kV. The direction and shape of the beam is controlled by magnetic field. The material is loaded in a crucible and heated up by the e-beam, and evaporated. The material is thrown upward, towards the loading chamber where the sample is located. A shutter is used to control the deposition time of material. Deposition rate is controlled by the e-beam current. The sample can be tilted if needed, to improve the electrical contact to the interface.

The pressure of the chamber is maintained at  $< 10^{-6} \text{ Torr}$  to avoid any oxidation of material during deposition. Also, when titanium is used to make contact between gold bonding pads and LAO/STO interface, a pre-deposition evaporation of 10 minutes is required. The evaporated titanium can trap the remaining oxygen molecules in the chamber, and further reduce the oxidation on the target metals.

### 4. Lift-off

When the sample is patterned with photolithography and coated with metal, the photoresist and the excessive metal need to be removed. Photoresist can dissolve in organic solvents such as acetone. Acetone has high vapor pressure, so it is not suitable to be heated up to increase solubility of photoresist. Also, when acetone dries up on sample it forms streaks. Therefore the sample needs washed with IPA to remove the acetone residue. When the photoresist

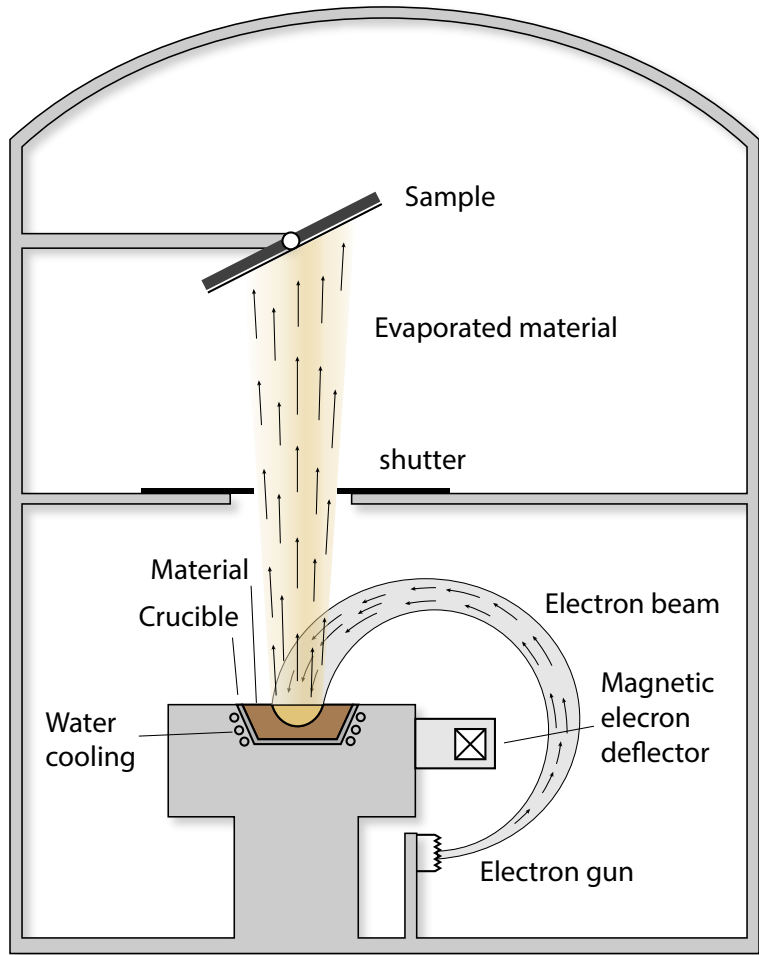


Figure 14: E-beam evaporator. The electron beam is generated from an electron gun on the bottom. The beam is deviated and shaped by magnetic field, towards the material. Them material is loaded in a crucible and heated up to melting point. The vapor of the material is thrown towards the sample on top. Deposition time is controlled by a shutter.

is heated up to 140 °C, it will cross-link and its solubility in will decrease. 1165 remover (1-methyl-2-pyrrolidone, or NMP) need to be used for lift-off in such cases. It has low vapor pressure and can be heated up to 80 °C. If 1165 still cannot fully remove the photoresist after sample is immersed in it for 24 hours, oxygen plasma cleaner is needed.

## 5. Oxygen plasma cleaning

The oxygen plasma cleaner activates oxygen molecules with a high frequency voltage (kHz to MHz) in low pressure, and forms plasma or oxygen radicals when electrons recombine with oxygen ions. The mixture is highly reactive and interactive with organic materials like photoresist residue on sample surface. Oxygen plasma cleaning can be categorized as a form of RIE (as discussed in Section II.B.2), but it usually operates at high end of 100 mTorr and the etching is less directional. Compared to chemical solvent, oxygen plasma removes the photoresist residue at a much lower speed (about 10 nm/min), but the finishing is much cleaner, while less invasive compared to RIE. Therefore, oxygen plasma is used as a final step for sample processing.

## C. ELECTRONIC SIGNAL MEASUREMENT

1. Lock-in amplifier
2. Virtual lock-in amplifier
3. IV-curve measurement

## D. ATOMIC FORCE MICROSCOPE

The atomic force microscope (AFM) is a type of instrument that uses a nanoscale probe to interact with the surface, and characterize the properties (topography, coulomb interaction, conductivity, etc) of a sample. It was invented in IBM lab by Bin, Quate and Gerber [1] in 1986 and later commercialized in 1989. The development of AFM technology benefited

from the advancement of STM and precise closed-loop spatial control using piezoelectric effect. However, AFM was invented to overcome the drawback of STM — only conductive or semi-conductive samples can be measured. AFM can measure various types of interaction between the probe and surface, such as surface potential, magnetic force, Van de Waals force, etc. Also, unlike the scanning electron microscopy (SEM) or tunneling electron microscopy (TEM), the AFM can be operated in various environment (aqueous, ambient, vacuum or cryogenic), and does not require the sample to be pre-treated (such as metal coating) or being conductive. The robustness and non-invasive nature of AFM make it a powerful tool for studying surface phenomena including charge density, magnetic dipole moment, capacitance, chemical bonding, nano-device lithography, and even biomacromolecules. AFM can also be integrated with other techniques, such as infrared spectroscopy[6]. The limitation of AFM is that the imaging cannot be as fast as SEM or TEM, as it relies on the physical movement of the tip.

## 1. Working principle

The AFM is mainly consist of three parts, as shown in Figure 15, AFM tip, laser optics, and piezoelectric scanning system. The AFM tip has a sharp end, with a radius of curvature in nanometer scale. A laser is reflected from the top surface the AFM tip and collected by a quad detector. The quad detector determines the position by

$$\begin{aligned} I_{\text{sum}} &= I_A + I_B + I_C + I_D \\ I_{\text{vdiff}} &= (I_A + I_B) - (I_C + I_D) \\ I_{\text{hdif}} &= (I_A + I_C) - (I_B + I_D), \end{aligned} \tag{II.1}$$

where  $I_A$ ,  $I_B$ ,  $I_C$  and  $I_D$  are the intensities on the four quadrants of the detector.  $I_{\text{sum}}$  is the total intensity.  $I_{\text{hdif}}$  and  $I_{\text{vdiff}}$  are the horizontal difference and vertical intensity difference. Assume the laser spot has Gaussian distribution. When the center of laser spot changes, the distribution of intensity on the four quadrant would change. The detector can monitor the movement by the horizontal and vertical differences in intensities.

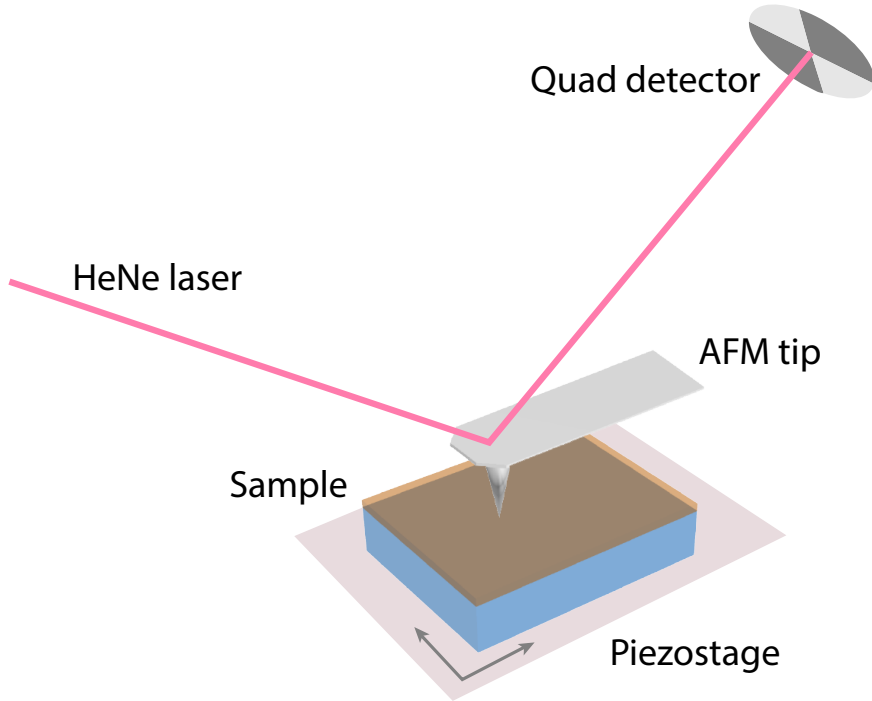


Figure 15: The schematics of AFM. A laser is reflected from the top surface of the AFM tip, and collected by a quad detector. A small amount of deformation would cause the center of laser spot to move on the quad detector, and measured as a change of differential voltage.

When the interaction between the tip and sample surface changes and the tip is slightly deformed, the laser spot would move on the quad detector. The deformation of tip follows Hooke's law:

$$F = -k \cdot x$$

Where  $x$  is the amount deformation, and  $k$  is the spring constant of the tip cantilever.  $k$  is mostly between 1 N/m and 100 N/m, depends on the type of the tip. In my experiment I use tips with spring constant  $k = 3$  N/m. The interaction between the AFM tip and sample surface is a function of distance. The attractive interaction decays slower than the repulsive interaction, therefore the total interaction follows the curve in Figure 16.

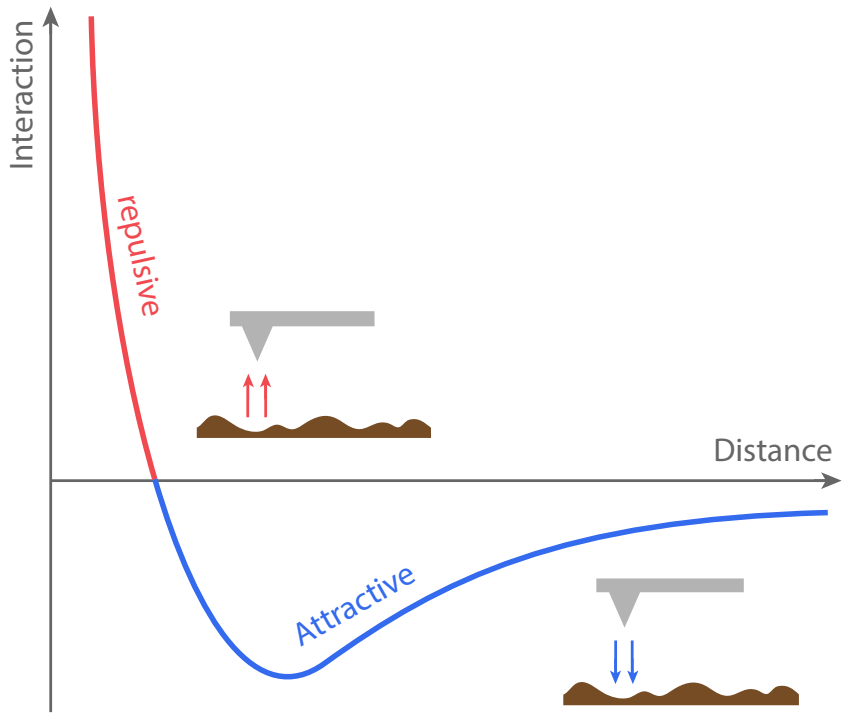


Figure 16: The interaction between tip and the sample surface. At long distance the interaction zero. When the tip moves towards the sample, the interaction is attractive. As the tip gets closer, the interaction would switch from attraction to repulsion, and gets larger and larger the tip moves closer.

The sample is located on the piezoelectric scanning stage. The movement of the sample and the tip, and signal from the laser optics system are controlled and monitored by a computer. The type of signal depends on the working mode of AFM and nature of the interaction it is targeting. More details are discussed in the following sections.

## 2. Contact mode

In contact mode, the AFM tip is in close contact with the sample. The distance between the tip and sample is controlled by a piezoelectric actuator. As shown in Figure 17, When the tip

approaches the sample surface, repulsion from the sample would deform the tip and changes the reflection angle of laser spot. The intensity difference on the quad detector would also change, in terms of a voltage signal. When the sample is driven by the piezostage and cause the tip moves relative to the sample, the repulsive force between the tip and sample surface is regulated by a feedback loop between voltage on the piezoelectric actuator, and the voltage difference on the quad detector, so that the amount of tip deformation and repulsive force is a constant.

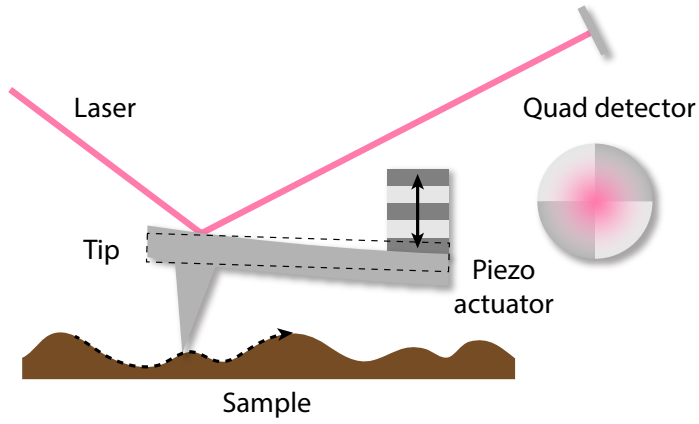


Figure 17: AFM contact mode. The tip is pressed to the sample surface by the piezoelectric actuator. The deformation of the tip is monitored by the quad detector. The voltage of the piezoelectric actuator is controlled with a feedback loop with the deflection voltage on the quad detector.

### 3. AC mode

In AC mode, the AFM tip is driven by a sinusoidal electrical signal on the tip piezoelectric actuator, as shown in Figure 18. The electric frequency is close to the resonance frequency of the tip (10 kHz - 500 kHz). The driving frequency is not exactly at the resonance frequency, so that the gradient of amplitude change is maximized and the system is most sensitive to the interaction change. The laser spot and difference signal also oscillates at the same frequency. When the tip approaches the sample surface, the interaction between the tip and

surface will cause the resonance frequency to shift and change the amplitude  $A$  and phase  $\theta$  of the tip oscillation and monitored by the differential voltage signal on the quad detector. The measurement can be integrated with lock-in amplifier technique (more discussion can be seen in section ??) for noise reduction. When the tip scan through the surface,  $A$  and  $\theta$  are recorded for each position on the sample surface and mapped onto a 2D image. The voltage on the piezoelectric actuator ( $z$  voltage) is controlled by a feedback loop so that the amplitude  $A$  is maintained at a set point. During the scan the tip is not continuously in contact with the sample surface, but “tapping” the sample with oscillations, therefore AC mode is sometimes called “tapping mode”. Compared to contact mode, in the AC mode the tip does not scratch the sample surface, so it has less effect on the sample.

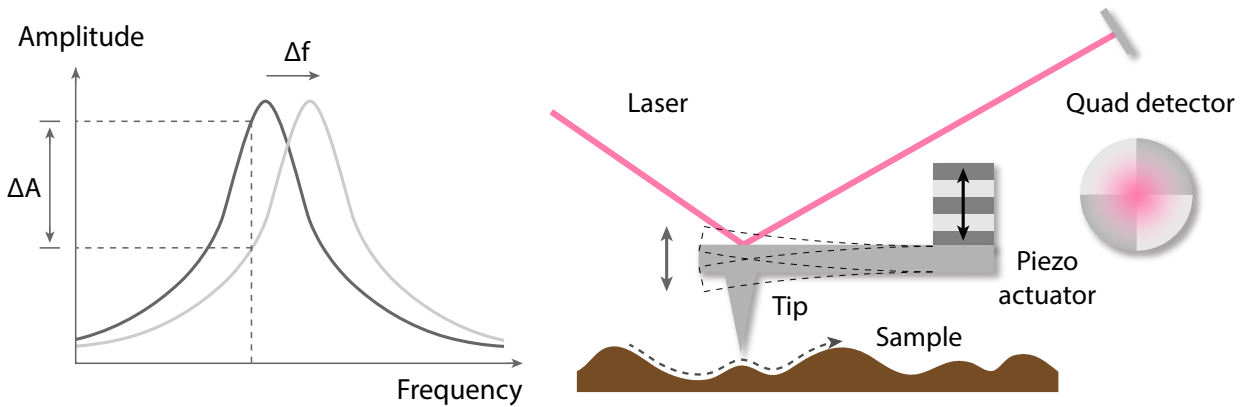


Figure 18: AFM AC mode. Left: the tip is driven at a frequency close to the resonance frequency. When the resonance frequency shifts as the interaction between the tip and the sample changes, the Change of oscillation amplitude is monitored by the quad detector and sent to the computer.

#### 4. Non-contact mode

In the non-contact mode, the tip is maintained at the attractive regime so that the sample does not have direct contact with the tip. The tip and the sample is maintained at distance

that the interaction is always attractive while the tip is scanning through the sample (Figure 19). This is especially important for biomacromolecules and organism.

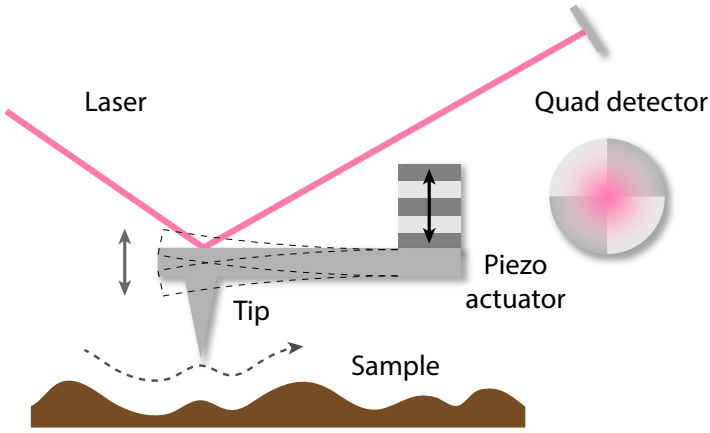


Figure 19: AFM Contact mode. The tip is kept at a distance from the sample so that the interaction is always attractive. The tip does not have direct contact with the sample during the scanning.

## 5. Magnetic force microscopy

When the tip is coated with ferromagnetic materials (e.g. Co, Fe), the AFM is able to measure the magnetic interaction with magnetic force microscopy (MFM). Similar to AC mode, the tip is driven by an oscillating AC voltage close to the resonance frequency (about 100 kHz in my experiments), and the change of interaction is monitored by the amplitude  $A$  and phase  $\theta$  of the differential voltage on quad detector. The challenge of MFM is that the magnetic and Van der Waals interactions are coupled together. The two-pass technique is used to solve this problem, considering that Van der Waals interaction is short-ranged and decays much faster than the magnetic interaction. First, the tip scans the sample close to the surface, and measures the topography. Second, the tip is lifted and maintained at a constant distance (such as 50 nm) from the sample surface using the height information obtained from the previous scan, so that the Van der Waals interaction is negligible, and the

spatial gradient of magnetic force can be measured[?]:

$$\Delta A \approx \frac{2A_0Q}{3\sqrt{3}k} \cdot \frac{\partial F_z}{\partial z}, \quad \Delta\phi \approx \frac{Q}{k} \cdot \frac{\partial F_z}{\partial z}, \quad \Delta f \approx -\frac{f_0}{2k} \cdot \frac{\partial F_z}{\partial z}, \quad (\text{II.2})$$

where  $\Delta A$ ,  $\Delta\phi$  and  $\Delta f$  are the change of amplitude, phase and resonance frequency;  $A_0$  and  $f_0$  are the original amplitude and frequency;  $Q$  and  $k$  are the resonance quality factor and cantilever spring constant.  $\partial F_z/\partial z$  is the spatial gradient of magnetic force.

Like contact and AC mode of AFM, the resolution of MFM is limited by the tip radius of curvature. Ferromagnetic coating of the MFM tip is about 40 nm in my experiments, so the resolution is in the same order of magnitude.

The advantage of MFM is that, the resolution and sensitivity is higher than other methods such as magneto-optical effect imaging. Also, like contact and AC mode AFM imaging, MFM does not require special treatment on the sample. The downside of MFM is that the imaging speed is limited by the raster scanning speed. The two-pass method takes twice as long as usual AFM AC scanning. Also, as equation (II.2) shows, MFM signal is not determined by the absolute value of magnetic force, but is proportional to the spatial gradient of the force  $\partial F_z/\partial z$ , therefore the scanning speed would also affecting the signal. The field from the AFM tip can also affect the magnetic dipoles on the sample, and MFM image can change after each scan. Other long range interaction such as coulomb interaction cannot be eliminated by the two-pass method, and need to be taken care of. More details are discussed in the next chapter. In spite of these disadvantages, the MFM is still a power tool to study surface magnetism for its robustness and simplicity of operations.

## 6. Piezoresponse force microscopy

The high sensitivity and extendability of AFM make it a versatile tool to measure different types of interactions between the tip and sample. One important variant is piezoresonse force microscopy (PFM). Piezoelectric effect is the phenomenon when an external stress or strain is applied to a piezoelectric material, the deformation will induce electric dipole moments and build up an internal electric potential across the sample. Inversely, the external electric

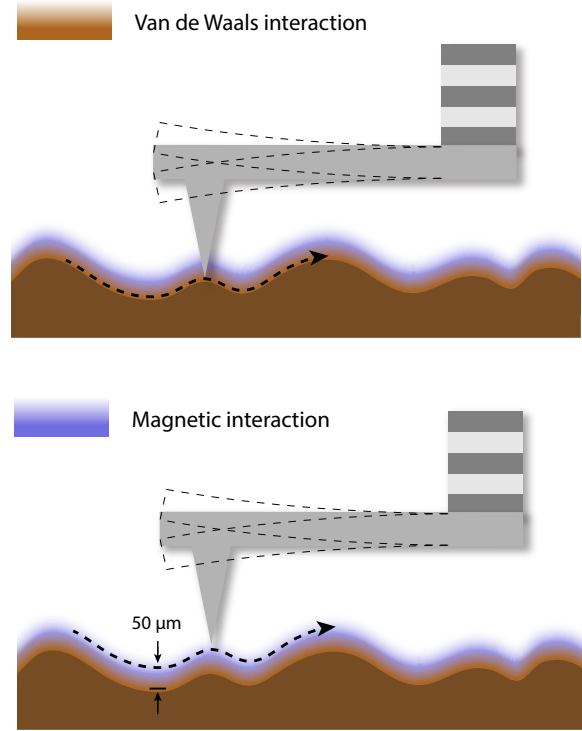


Figure 20: MFM mode. The first scan is close to the sample surface, so that the topographical information can be obtained. In the second scan the tip is lifted to a constant distance from the sample surface, so that the Van der Waals interaction is negligible and only the long-ranged magnetic interaction is measured.

field can also induce mechanical deformation. Depending on the properties of the material, the deformation can be either expansion or contraction. The effect can be described with

$$X_i = d_{ki} E_k,$$

where  $X_i$  is the strain tensor,  $d_{ki}$  is the piezoelectric tensor and  $E_k$  is the electric field. For a tetragonal system,

$$\begin{bmatrix} X_1 \\ X_2 \\ X_3 \\ X_4 \\ X_5 \\ X_6 \end{bmatrix} = \begin{bmatrix} 0 & 0 & d_{31} \\ 0 & 0 & d_{32} \\ 0 & 0 & d_{33} \\ 0 & d_{15} & 0 \\ d_{15} & 0 & 0 \\ 0 & 0 & 0 \end{bmatrix} \begin{bmatrix} E_1 \\ E_2 \\ E_3 \end{bmatrix}$$

When a field is applied in  $E_3$  direction, the resulting non-zero strain terms are  $X_1 = d_{31}E_3$ ,  $X_2 = d_{32}E_3$  and  $X_3 = d_{33}E_3$ . Therefore, an electric field in the c-axis of the crystal will cause elongation in the c-axis and contraction in the other two orthogonal directions, or vice versa. The piezoresponse of sample can bring insights of the sample properties such as carrier concentration[], ferroelectric domain orientation[], domain boundary[], etc.

In PFM measurement, a conductive tip made of doped silicon or coated with metal is in contact with the sample and a sinusoidal voltage signal is applied to the tip. For a sample with piezoresponse, the electric field will cause a deformation of the sample topography sinusoidal in time. Since the sample is in contact with the tip, the topographical change of sample will cause slight change of tip deformation and the change is recorded by the differential voltage on the quad detector. The sample deformation is usually in the order of 10 pm/V (e.g. 85.6 pm/V for BaTiO<sub>3</sub>[]). Therefore, PFM signal is measured with lock-in technique for the best signal-to-noise ratio. As shown in Figure 21, If the sample contract in the direction of the electric field, the piezoresponse signal will be in phase with the electric signal; if the sample elongate in the direction of the field, the signal will be out of phase.

## 7. LAO/STO nano-device c-AFM lithography

### E. GRAPHENE/LAO/STO DEVICE FABRICATION

Current state-of-the-art high quality graphene devices are fabricated from mechanically transferred exfoliated graphene encapsulated with hexagonal boron nitride (h-BN)[?], where the mean-free-path of the electron can exceed the dimension of the device[?] (tens of mi-

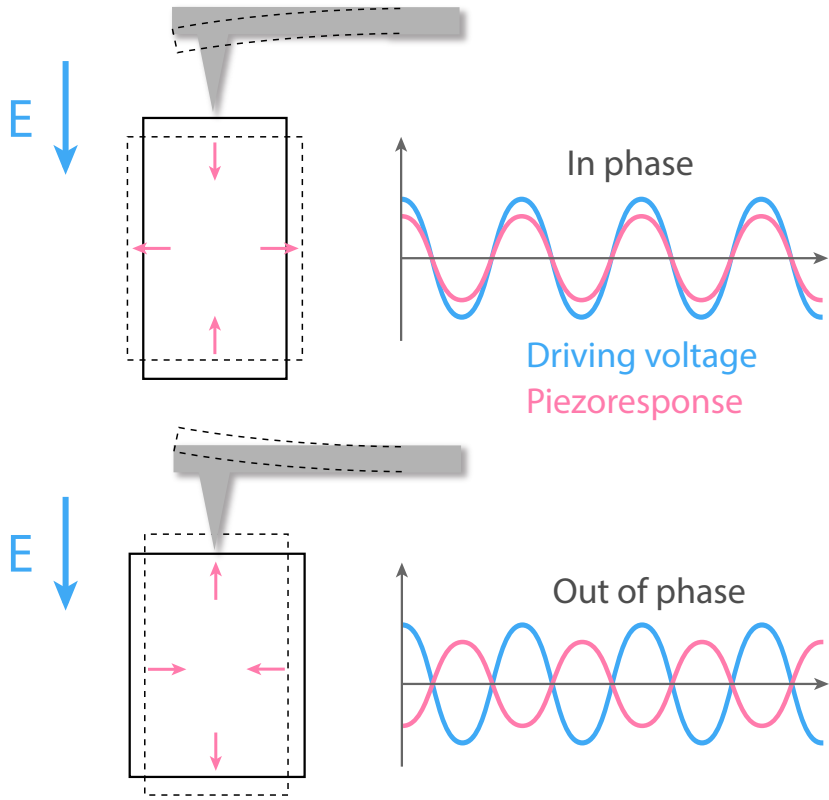


Figure 21: PFM measurement. The external electric field is applied on the sample through a conductive tip. The sample deforms and slightly bend the tip, and the deformation signal is monitored with a quad detector (not shown). If the sample contract in the direction of the field, the deformation signal is in phase with the driving voltage (above); if the sample elongate in the direction of the field, the signal would be out of phase with the driving voltage (below).

crometers). For applications requiring an arbitrary substrate and graphene shape like my experiment, graphene grown from CVD method and transfer in liquid (“wet-transfer”) is preferred. The basic idea of wet-transfer is to use wet chemical etchant such as nitric acid, hydrochloric acid,  $\text{FeCl}_3$  or ammonium persulfate (AP) to etch away the metal substrate while the graphene is floating on the liquid surface. The graphene is then scooped out and rinsed in DI-water for several times while floating on water. The substrate is then immersed

in the DI-water and used to catch the graphene piece from the bottom. Conventionally, the wet-transfer needs polymers like poly(methyl methacrylate) (PMMA) a scaffold layer to support graphene on the liquid surface before it is transferred onto the substrate[?, ?, ?]. The PMMA is then patterned with deep UV exposure or e-beam lithography, so that graphene can be etched in to the designed shape. In the end the PMMA is cleaned with organic solvent. The procedure of using PMMA to transfer and pattern graphene shown in Figure 22.

The issue with PMMA as transfer medium is that, the residual PMMA is known to be a source of electron scattering, and would significantly reduce the electron mobilities[?, ?, ?]. Annealing the sample in H<sub>2</sub>/Ar environment proves to partially remove the residue, but the process can also introduce structural defects to graphene[?], or increase coupling between graphene and the substrate and result in extrinsic doping and deterioration of mobility[?].

Another drawback of using PMMA as a transfer medium is that LAO/STO substrate is susceptible to PMMA contaminants. Figure 23 shows the AFM AC phase image of LAO/STO with a graphene piece transferred and patterned with PMMA. The inside the circular region is graphene. On the LAO/STO surface, contamination particles can be seen. Many experiments in my project require tuning the 2D electron gas on the interface of LAO/STO with c-AFM (will be discussed in Section II.D). Most of the LAO/STO samples were found to lost the interface tunability after the graphene transfer with PMMA.

A replacement we found for PMMA is a type of perfluoropolymer Hyflon from Solvay. Our collaborator Brian D'Urso has used Hyflon for hydrodynamic experiment, and suggested it might work as a perfect protection layer for graphene. Hyflon is a type of perfluorinated polymer (similar to Teflon), and is highly hydrophobic and chemically stable. Hyflon has been reported to be widely used in membrane applications such as fuel cells, due to the inertness of C-F bonds[?, ?, ?]. It has also been reported that the Hyflon membrane between graphene and substrates like SiO<sub>2</sub> can reduce the extrinsic p-type doping in graphene by preventing water molecule adsorption to the dangling bonds on the substrates[?]. It means that, unlike PMMA that leaves residue and deteriorate graphene quality, Hyflon can actually preserve the graphene while used as a transfer medium. Hyflon is also high selectivity to solvent.

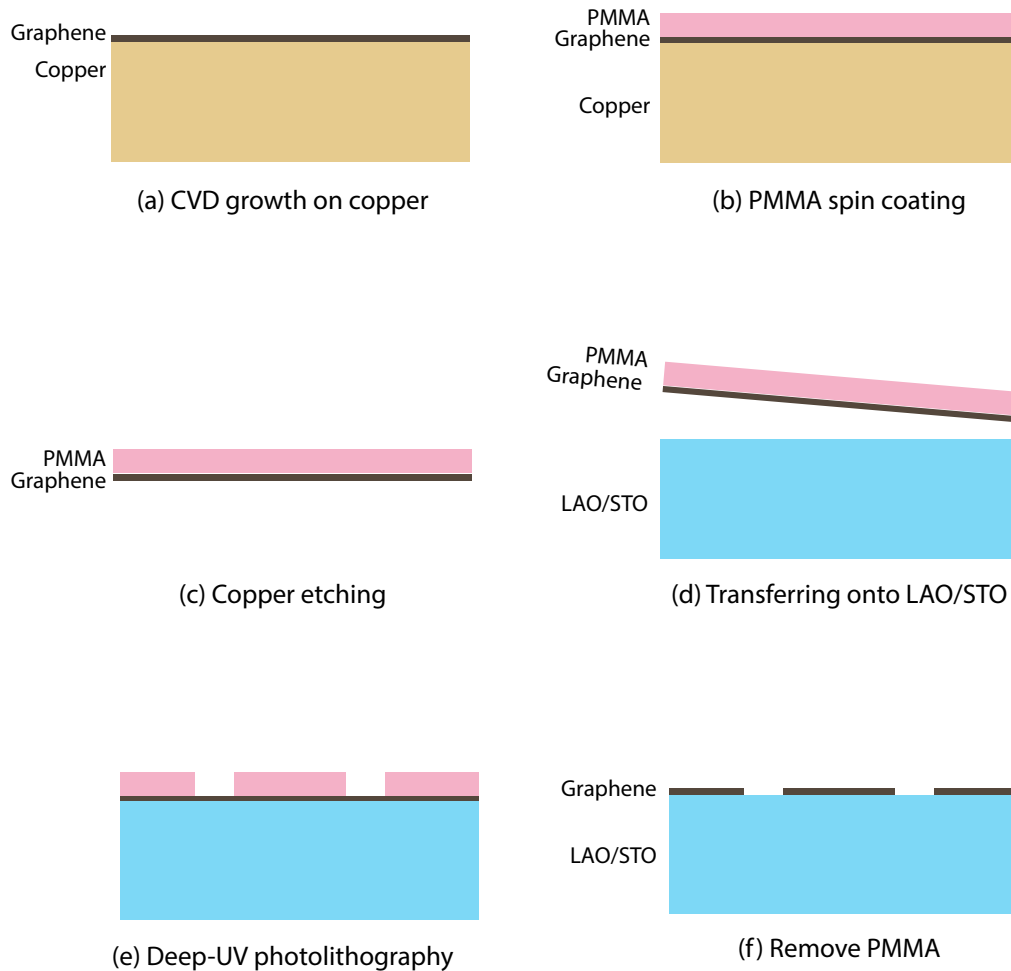


Figure 22: CVD graphene transfer and patterning with PMMA. (a) Graphene is grown on copper with CVD. (b) PMMA is spin-coated onto graphene surface. (c) Copper is etched chemically, while graphene floats on the liquid surface. (d) Graphene is transferred onto LAO/STO, using PMMA as a supporting layer. (d) PMMA is patterned with deep-UV lithography. (f) PMMA is removed with organic solvent.

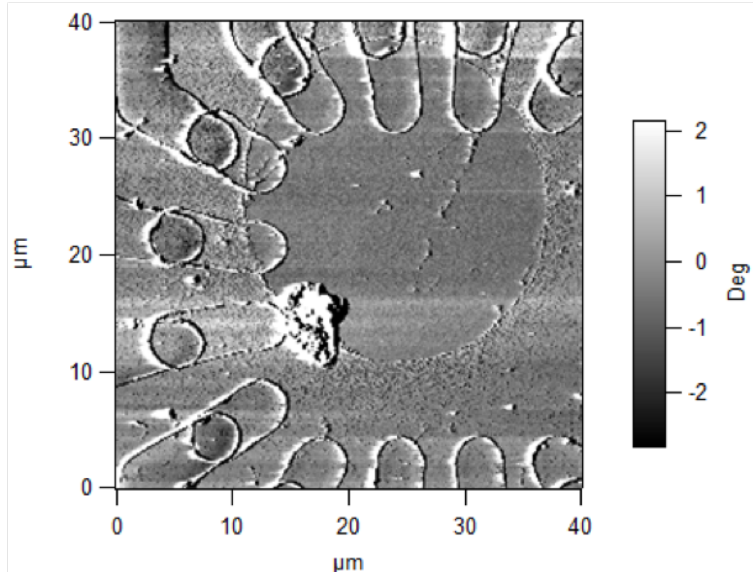


Figure 23: AFM phase image of graphene on LAO/STO, transferred with PMMA. The circular region is graphene. Particles can be seen outside graphene, on LAO/STO surface. Other features are the metal electrodes for graphene and interface contact.

Most of the organic or inorganic solvent such as acetone, IPA or DI-water cannot dissolve Hyflon, which makes it a perfect protection layer for graphene.

The commercially available Hyflon is in powder form. It is only soluble in a few types of perfluorinated solvent. In my experiment I used FC-40 to make Hyflon solutions. There are different types of Hyflon available, mainly Hyflon AD 40 and Hyflon AD 60, with different molecular weights and phase transition temperature. I have tested both types, and found that graphene transferred with Hyflon AD 60 has higher quality. Although AD 40 has smaller molecular weight and easier to be dissolved, the sample soft-baking temperature is higher than the phase transition temperature of AD 40, and would cause cross-linking of the polymer chains. This makes Hyflon AD 40 hard to be removed and affects graphene quality as a result.

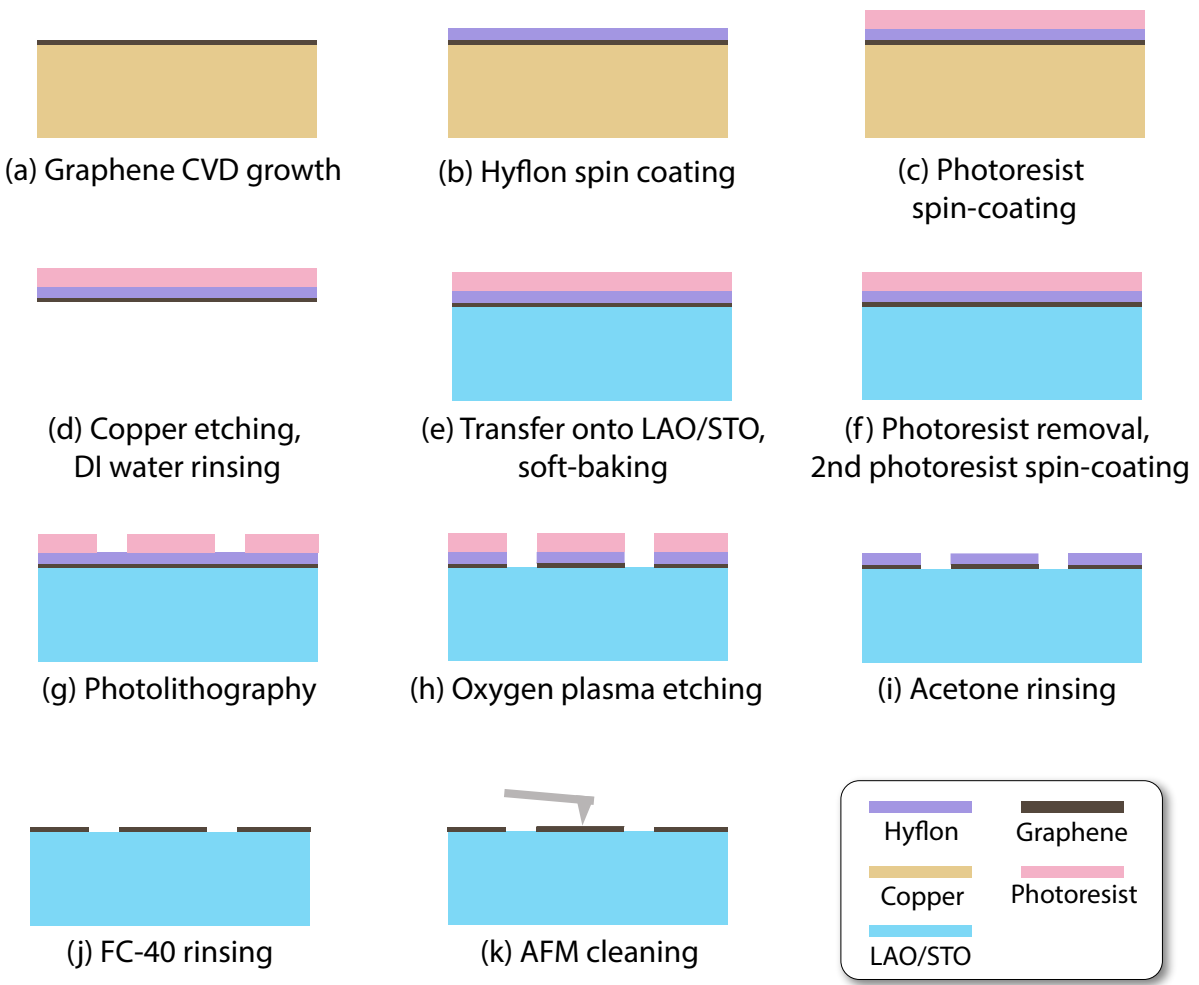


Figure 24: Hyflon transfer and patterning procedure. (a) Graphene is grown with CVD on a copper substrate. (b) Hyflon is spin-coated on graphene. (c) A layer of photoresist is coated on Hyflon as a supporting layer for wet-transfer. (d) Copper substrate is etched with ammonium persulphate; graphene is rinsed in DI-water for several times. (e) Graphene is transferred onto LAO/STO surface. (f) Photoresist for transfer assistance is removed; another layer of photoresist is coated. (g) Standard UV photolithography. (h) Oxygen plasma etching on the excessive graphene. (i) Photoresist removal with acetone. (j) Hyflon removal with FC-40. (k) Residue particle cleaning with AFM.

## **1. Overview of the Hyflon transfer method**

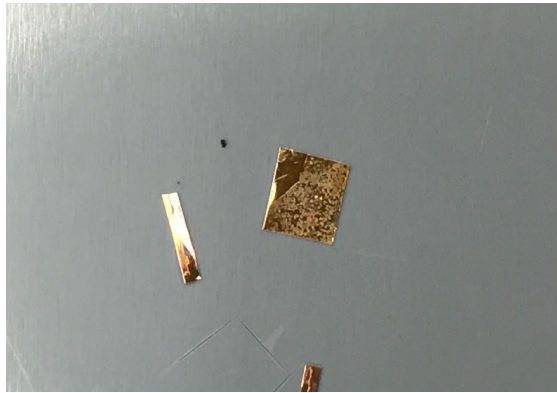
The procedure for graphene transfer with Hyflon is similar to the PMMA transfer method. As shown in Figure 24, the graphene on copper is spin coated with Hyflon. The Hyflon film is only 50 nm, therefore a second supporting layer, photoresist, is spin-coated on top of the Hyflon. The copper is etched with ammonium persulphate while graphene with Hyflon and photoresist floats on the surface of chemical. The graphene is then rinsed 4 to 5 times and then transferred onto a pre-patterned LAO/STO substrate, and soft-baked to remove the DI water between graphene and LAO. The photoresist is then removed, and another layer of photoresist is spin-coated. The sample is patterned into Hall bars with standard photolithography. Excessive graphene is etched away with oxygen plasma, along with the Hyflon covering it. The patterned graphene/LAO/STO sample is rinsed with acetone to remove the photoresist, and then Hyflon is removed with FC-40. The particles left on the patterned graphene surface is cleaned by AFM in contact mode scans.

## **2. Hyflon solution preparation and spin-coating**

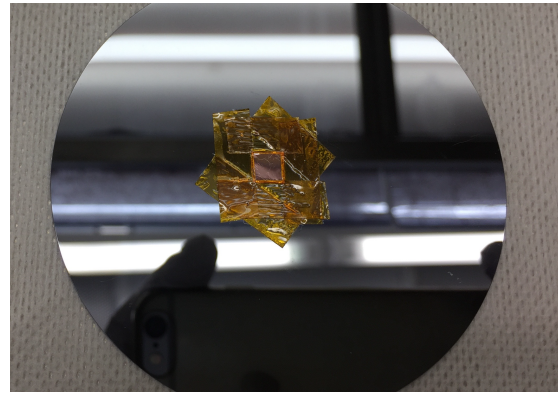
Hyflon solutions in FC-40 are made by adding 2.5 grams of Hyflon powder into 100 ml FC-40 (nominally 2.5%). The solution is shaken at 100 rpm for 48 hours. Before spin-coated on sample, the Hyflon solution needs go through a series of filters of 450 nm, 200 nm and 100 nm in size to remove any undissolved particles. When spin-coated at 3500 rpm, the thickness of Hyflon film is about 50 nm. In the past we also used 0.5% Hyflon solution and spin-coated at 1000 rpm to make coatings of 50 nm, but it turned out that higher concentration of Hyflon solutions spin-coated at a higher speed would yield more uniform films on graphene samples.

## **3. Graphene preparation, copper etching and wet transfer**

The as-grown CVD graphene is on 100  $\mu\text{m}$  thick circular copper foil. The LAO/STO substrates that graphene will be transferred on are 5 mm  $\times$  5 mm squares. Therefore, the graphene on copper needs to be cut into 5 mm  $\times$  5 mm shape with a razor blade as shown in Figure 25(a). Graphene single domains can be seen in the Figure. The square shape copper



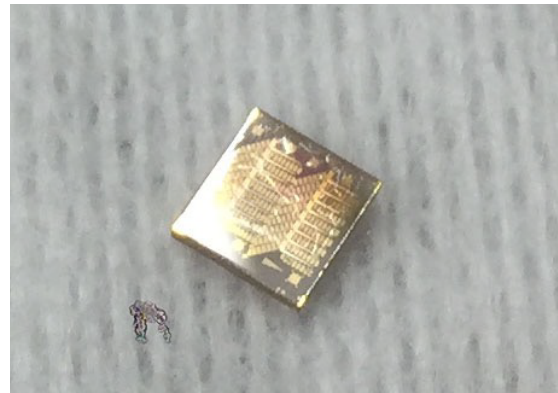
(a)



(b)



(c)



(d)

Figure 25: (a) The graphene with copper foil is cut into squares. The graphene single domains can be seen. (b) copper foil with CVD graphene is fixed onto a silicon wafer as a spin-coating carrier. The edges of the copper foils are carefully sealed with Kapton tape to prevent Hyflon solution leaking into the space between copper and silicon substrate. (c) After the copper is fully etched by ammonium persulfate, the graphene flake with Hyflon and photoresist floats on the surface of the liquid. (d) Graphene transferred onto pre-patterned LAO/STO. Liquid between the graphene LAO is evaporated in an oven or on a hot plate.

foil is then fixed onto a 3" silicon wafer for spin coating, with Kapton tapes, prepared for Hyflon spin coating. The edges of the graphene need to be carefully sealed, so that the Hyflon solution will not leak into the space between the copper and silicon wafer. In the past, we used to leave the edges open, and the Hyflon will be left on the backside of the copper. After copper etching and graphene transferred onto the LAO/STO, the Hyflon on the backside will be trapped between graphene and substrate and impossible to be removed.

Transferring graphene with only the 50 nm Hyflon proved to be very hard. To address this issue, an additional layer of AZ4210 photoresist is spin-coated on Hyflon. However, since the Hyflon is highly hydrophobic, the photoresist solution cannot stick to the surface and form a film of  $2.1\mu\text{m}$  thick, as it usually does on hydrophilic surfaces. A mild oxygen plasma etching is performed to modified the Hyflon surface and improve surface hydrophilicity. The parameters of plasma etching need to be carefully tested. Etching will not only change the Hyflon hydrophilicity, but also change the solubility of Hyflon in FC-40. In the last step where Hyflon is removed by FC-40 from graphene, if the previous Hyflon surface treatment is too strong, the modified Hyflon can cross-linked and hard to be fully removed from graphene. In practice, etching the Hyflon for only a few nanometers would drastically improve the hydrophilicity and make photoresist spin-coating possible.

After spin coating, the copper foil is taken off the silicon substrate. 1 mol/L concentration ammonium persulfate ( $(\text{NH}_4)_2\text{S}_2\text{O}_8$ ) DI-water solution is prepared beforehand. Ammonium persulfate is a type of oxidation agent widely used as copper etchant in printed circuit board industry. Compared to other chemicals like ferric chloride, ammonium persulfate does not leave metal ion to graphene, which is critical for experiments on magnetism or transport. The ammonium persulfate solution also needs to go through a 450 nm polymer filter before the copper foil is place on the surface of it. Copper etching usually takes 3-4 hours.

After the graphene transferred onto the LAO/STO, we sometimes found that the sample was dirty, and the contaminants seemed to be introduced by the transfer procedure. AFM scanning showed that the contaminants were trapped between graphene and LAO. One possibility was that the contaminants were the graphene grown on the backside of the copper. When the copper was etched away by ammonium persulfate, the backside graphene did not sinked into the etchant, but transferred with the topside graphene onto the sample and got



Figure 26: (a) Without copper substrate backside cleaning, the graphene transferred onto LAO/STO has contaminant trapped. (b) The graphene on LAO/STO is much cleaner if the backside is cleaned.

trapped between graphene and LAO.

The two-step etching procedure can be used instead. After the copper top surface is coated with Hyflon, it is placed on the surface of ammonium persulfate solution and left inside an ultrasonic cleaner for 15 minutes. While the backside of the copper is been etched, it is also scratched by the ultrasound wave so that the backside graphene can be removed. After 15 minutes, the backside is washed by spraying DI-water on it. The graphene on the topside is protected by Hyflon, and will not be affected by the backside cleaning. Then the copper foil is placed back on the surface of ammonium persulfate. After 3-4 hours the copper foil is fully etched, and the graphene with Hyflon and photoresist would float on the surface, as shown in Figure 25(c). The gray color of the floating flake is from the AZ4210 photoresist. The dark spot on the lower-left corner of the flake is a piece of contaminant.

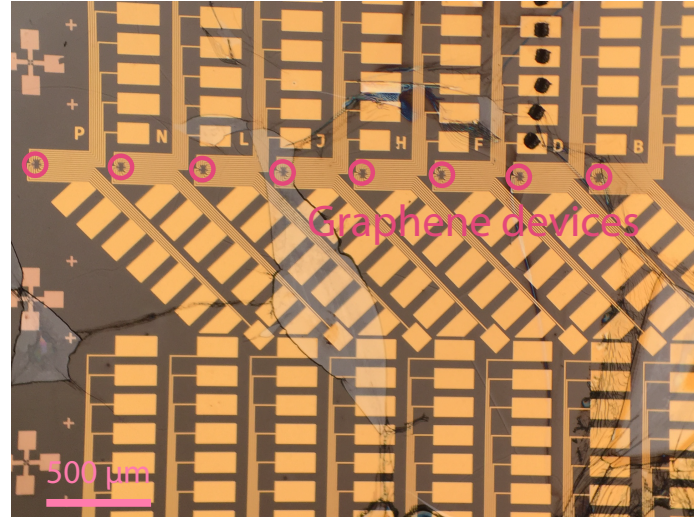
The graphene flake is then scooped out with e mesh and place on the surface of DI-water, repeated for 4-5 times to make sure the ammonium persulfate is washed off the backside of

the flake. Then the LAO/STO substrate is immersed in the DI-water where the flake is floating. The substrate is slowly lifted up towards the flake on the liquid surface, and catch the flake when it comes out of the water. The substrate with the graphene flake on surface is then baked in an oven pre-heated to 50°C, or on a hot plate at 70°C for 5–10 minutes so that the DI-water between graphene and substrate is evaporated and graphene firmly adheres to LAO (Figure 25(d)).

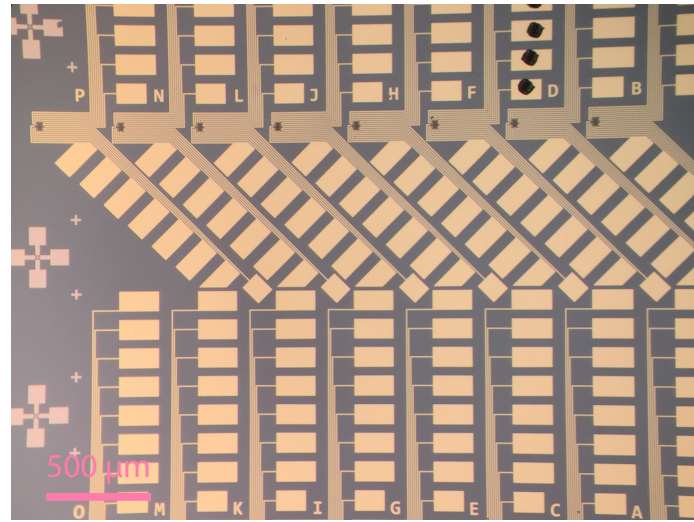
#### 4. Photolithography and etching

The graphene transferred onto LAO/STO is patterned with standard UV photolithography, as discussed in Section II.B.1. Although there is already photoresist on graphene flake to assist wet transfer, it needs to be washed off and re-coated, because it is exposed to UV and chemical etchant. Unlike the photolithography for LAO/STO electrodes, patterning graphene into Hall bars need to wash off the photoresist outside of the Hall bars and leave the Hall bar region covered with photoresist, so that the graphene is protected from oxygen plasma etching. The oxygen plasma barrel etcher and RIE proved to be effective for patterning graphene. However, other than the Hyflon and graphene, there are usually contaminant introduced by wet-transfer procedure that need to be cleaned with RIE as well (Figure 27).

**a. One-step etching** Before 2018 I was using the one-step etching method, that is to etch the graphene and clean the contaminants with RIE in one step. Figure 27 shows the image of a sample before and after the RIE etching. In Figure 27(a), it can be seen that bubbles or foldings introduced from the wet transfer covers the entire sample. Fortunately in my experiments, most of the graphene transferred on LAO/STO needs to be etched away, and only the graphene device inside red circles in 27(a) need to be covered with graphene. A zoomed-in image is shown in Figure 28, with graphene covered with Hyflon. The metal patterns are contact electrodes for graphene and LAO/STO interface. Wrinkles on graphene can be seen, which are following the corrugations on the copper substrate during CVD growth. The patterns for the entire sample are designed in the way that there can be as many graphene devices fit in the sample as possible, so that there are higher chances of



(a)



(b)

Figure 27: Contaminants can be introduced by wet transfer. The source can be photoresist, copper etchant, or liquid trapped in the bubble formed from transferring. (a) Contaminants can be seen after graphene transfer. Only the graphene inside the red circles (zoomed-in image in Figure 28) need to be protected with photoresist, and rest of the graphene can be removed along with the contaminants by RIE procedure. (b) Sample surface is clean after RIE procedure.

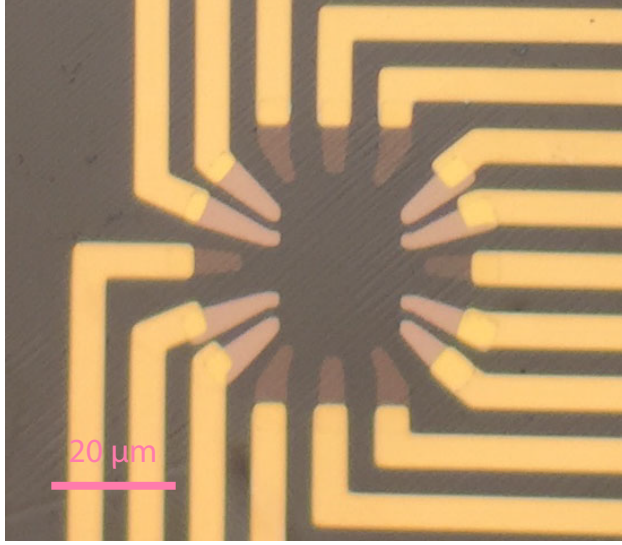


Figure 28: The graphene area of interest on pre-patterned LAO/STO sample. The patterns are for graphene and LAO/STO interface contact.

finding a clean graphene device. The contaminants are etched away with an aggressive RIE procedure (listed in Table 4).

As shown in Figure 29(b), the single-step RIE etching can completely clean the contaminants on LAO/STO. However, the etching can be problematic for the LAO/STO interface. Figure 29 shows the pattern of the graphene Hall bar and the surrounding electrodes to graphene and interface. Outside the graphene region is the surface of LAO/STO. Most of my experiment involves switching the LAO/STO interface conductivity with conductive AFM tip (to be discussed in section II.D). In some experiments, I need to create conductive nanostructures inside the  $20 \mu\text{m}$  square region shown in Figure 29. When the sample is too dirty and requires long etching time with RIE, LAO/STO is exposed in oxygen plasma for long time, and the bombardment would damage the interface and make it impossible to switch the conductivity inside the square region.

**b. Two-step etching** To address the interface-damaging issue, I started to use the two-step etching method. The basic idea is to separate sample cleaning and graphene etching

| Instrument | RIE        |
|------------|------------|
| Gas        | Oxygen     |
| Flow rate  | 19 sccm    |
| Power      | 50 W       |
| Pressure   | 300 mTorr  |
| Time       | 60 - 180 s |

Table 4: One-step RIE etching recipe.

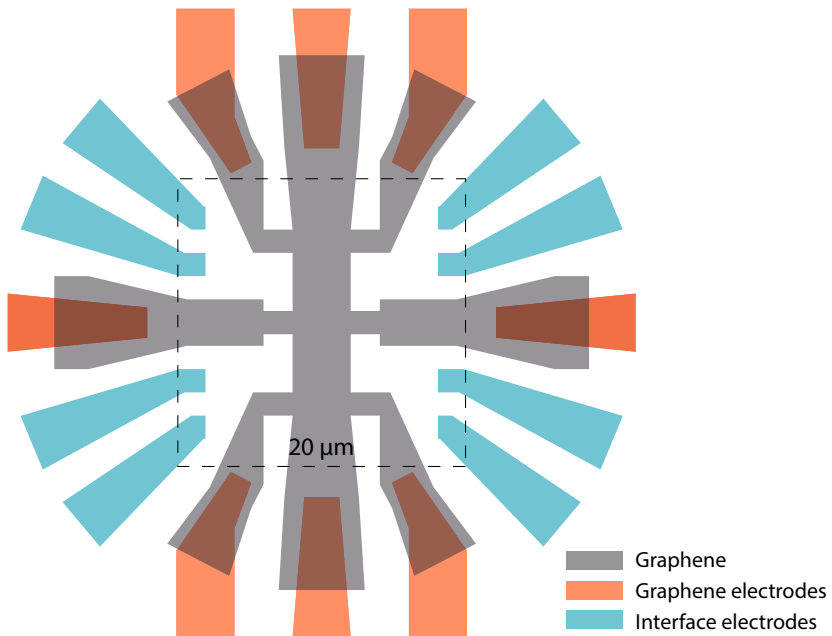
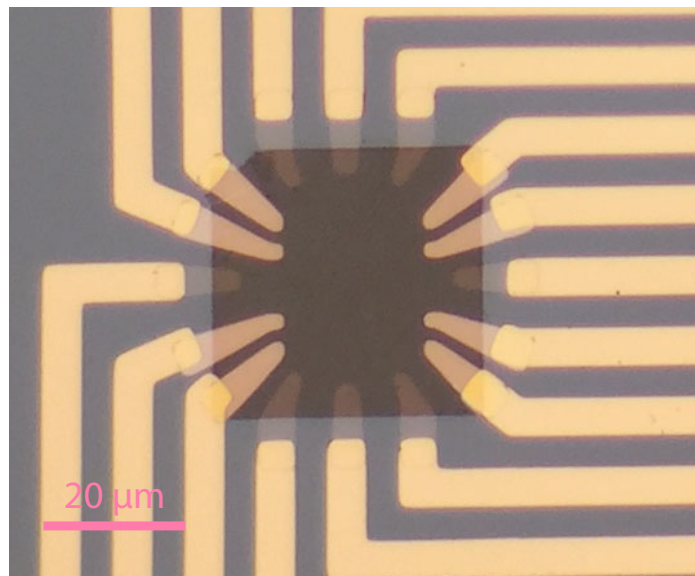
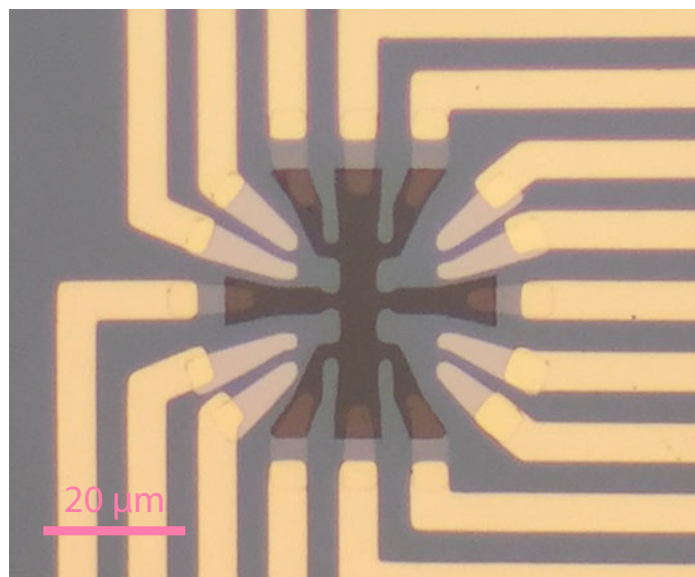


Figure 29: Graphene is shaped into Hall bars by RIE. Outside the Hall bar region, nanostructures need to be created inside the square region, on the interface of LAO/STO. Aggressive RIE process can damage the LAO/STO interface.

steps. As shown in Figure 30. In the first step of etching, the Hyflon and graphene are protected by photoresist in a square shape, that covers the Hall bar devices to be pattern



(a)



(b)

Figure 30: Two-step graphene etching.

in the next step and the LAO/STO canvas region. The rest of the sample is etch with an aggressive RIE step so that the contaminants on bonding pads and connection patterns are fully removed. After the etching the photoresist is washed away with acetone and IPA. In the second step, another layer of photoresist is spin-coated, and patterned into graphene Hall-bar device shape. Then the graphene and Hyflon outside the Hall bar region but covering the LAO/STO canvas are etched away with a much weaker oxygen plasma, so that the LAO/STO interface will not be damaged.

The detailed procedures are shown in Figure 31. Right after graphene is transferred onto LAO/STO and the supporting photoresist is washed off, it is spin-coated with AZ4210. The square-shape is patterned with photolithography to protect the canvas. Then the sample is etched with RIE, until all the contaminants are cleaned. In some cases, the contaminants needs long etching time, and photoresist may be etched through. Multiple photolithography and RIE etching steps will be needed. For the same reason, AZ4210 ( $2.1\mu\text{m}$  thick) is preferred than AZ4110 ( $1.1\mu\text{m}$  thick). After that, AZ4210 is washed off, and AZ4110 is spin-coated. Photolithography on AZ4110 has higher precision. One thing I noticed was that the developing time required for AZ4110 is much longer than usual, possibly because the previous RIE etching changed the surface hydrophilicity and make the exposed photoresist harder to be washed off. After the Hall bar is patterned with inverse pattern, the sample is etched with a weak oxygen plasma barrel etching recipe, and shape the graphene and Hyflon into Hall bars (Figure 30). The recipe for photolithography and etching are listed in Table 5 and Table 6.

To remove the Hyflon on graphene Hall bars, the sample is left in FC-40 heated up to 70 °C, and is shaken at 100 rpm for 18 - 24 hours. To reduce the impurities, the FC-40 would go through 450 nm, 200 nm and 100 nm size filters, before used for Hyflon removal.

## 5. Graphene/LAO/STO nano-device lithography



Figure 31: Two-step graphene etching. (a) AZ4210 is spin-coated on Hyflon. (b) The photoresist is patterned into square-shape protection layer for the canvas. (c) An aggressive RIE process is used to fully remove the contaminants outside the canvas. (a) to (c) might be repeated if necessary. (d) AZ4110 is spin-coated. (e) Hall bar shape is patterned, to protect the Hyflon and graphene on the regions of interest. (f) A weak oxygen plasma etching step is used to remove the unwanted Hyflon and graphene. (g) AZ110 is washed off by solvents. (h) Hyflon is removed by FC-40.

| Photoresist          | AZ4210 (step 1) | AZ4110 (step 2) |
|----------------------|-----------------|-----------------|
| Spin-coating         | 4000 rpm        | 4000 rpm        |
| Baking               | 95 °C           | 95 °C           |
| UV dose              | 170 mJ          | 100-120 mJ      |
| Developer : DI-water | 1 : 4           | 1 : 4           |
| Developing time      | 120 s           | 240 - 600 s     |

Table 5: One-step RIE etching recipe.

| Instrument | RIE (step 1) | Barrel etcher (step 2) |
|------------|--------------|------------------------|
| Gas        | Oxygen       | Oxygen                 |
| Pressure   | 300 mTorr    | ~ 600 mTorr            |
| Power      | 50 W         | 100 W                  |
| Time       | 200 - 400 s  | 300 s                  |

Table 6: RIE and barrel etching recipe. Although it seems that the barrel etcher is running at higher power, the structure of the instrument make the etching much less invasive compared to RIE.

### **III. GRAPHENE P-N JUNCTION EDGE-STATE ENGINEERING**

#### IV. GRAPHENE/LAO/STO SUPERLATTICE DEVICE

## **V. MAGNETO-OPTICAL KERR EFFECT ON LAO/STO INTERFACE**

### **A. MOTIVATION**

### **B. EXPERIMENTAL SETUP**

### **C. RESULTS**

## **VI. OUTLOOK**

## VII. CONCLUSIONS

## **BIBLIOGRAPHY**